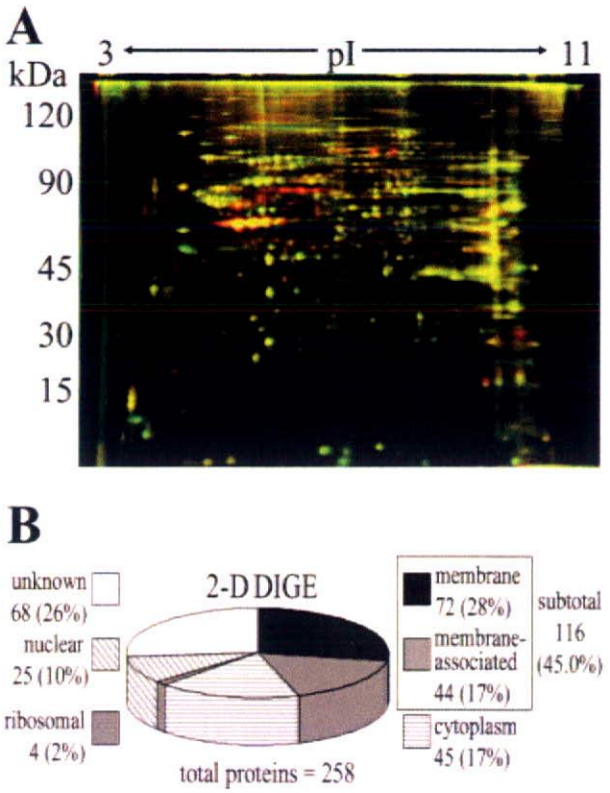

Figure 3. 2-D DIGE analysis of membrane proteins of pluripotent and differentiated murine ESCs. (A) A representative 2-D gel image. The green and red spots indicate undifferentiated and differentiated state-specific proteins, respectively. (B) Subcellular localization of proteins identified in the 2-D DIGE analysis.

technique (Fig. 3A and Supporting Information Fig. 1). Analysis with a fluorescence scanner detected 2488 spots. MS analysis of most of the differentially expressed protein spots and some of the other spots identified 258 unique proteins. The number of peptides used to identify a single protein ranged from 1 to 33, with an average of 6.1 peptides/protein, and 184 of the proteins (71%) were identified by multiple peptide assignments. The molecular masses (Mw) of the identified proteins ranged from 2.8 to 540 kDa, and the p*I* values ranged from 4.28 to 11.88. Some of the identified proteins were found in more than one spot, corresponding to proteins with similar Mw but different p*I* values, implicating the presence of post-transcriptional modifications, such as phosphorylation. After protein identification, the molecular and biological functions and subcellular localizations were annotated by searching the NCBI and Bioinformatic Harvester databases, and the numbers of transmembrane regions and potential secondary structures were predicted by the SOSUI software. A membrane protein has a signal sequence and/or more than one transmembrane region. In contrast, an intracellular membrane-associated protein has neither a signal sequence nor a transmembrane region, but it associates with membrane proteins. An extracellular membrane-associated protein has a signal sequence but no transmembrane region. Using these criteria, we classified 116 proteins as membrane and membrane-associated proteins (Fig. 3B and Supporting Information Table 1).

3.3 Shotgun-based analysis

For the quantitative analysis of membrane proteins derived from two different sources, isobaric labeling methods, including iTRAQ reagents, can be employed. We applied this method for the analysis of pluripotency-specific membrane proteins in murine ESCs. The purified membrane proteins were initially digested with trypsin, and the resulting peptides were labeled with iTRAQ, separated by HPLC, and subjected to MS/MS analysis. Although the peaks derived from two of the isotopic tags were indistinguishable in the MS analysis, upon tag fragmentation in MS/MS, peaks derived from the reporter tags (m/z = 114 and 117) were distinguished (Fig. 4A). The relative quantities of peptides prepared from the two different sources were compared based on the integration of peak areas.

For the efficient separation of iTRAQ-labeled peptide mixtures, we used 2-D LC with a combination of zwitterionic chromatography (ZIC-HILIC) and RPLC. In the first analysis, 10 315 MS/MS spectra were generated, while in the second round of analysis, 3500 MS/MS spectra were generated in which the first peak list was excluded. In these two analyses, the spectra were assigned to 2158 unique peptides by sequential MASCOT searching. All of these peptides were labeled with iTRAQ reagents. A total of 13 815 peptides were attributed to 659 unique proteins (Supporting Information Table 2). The number of peptides used to identify a single protein ranged from 1 to 32, with an average of 3.0 peptides/protein, and 339 of the proteins (51%) were identified by multiple peptide assignments. The Mw of identified protein sequences ranged from 5.3 to 876.5 kDa, and the p*I* values ranged from 4.18 to 12.57. Using the Bioinformatic Harvester database and the SOSUI software, 273 proteins were classified as membrane and membrane-associated proteins (Fig. 4B). In total, among 831 proteins identified by 2-D DIGE and 2-D LC methods, 338 proteins were classified as membrane proteins or membrane-associated proteins (Fig. 4C).

3.4 Verification of identified proteins

Some of the pluripotency-specific membrane proteins identified by MS (shown in Table 1) were verified by biochemical analyses. Whole lysates of murine ESCs cultured for 7 days with or without LIF were analyzed by Western blotting. As shown in Fig. 5A, the expression levels of various membrane proteins and membrane-associated proteins, such as Slc16a1, Akt2, ErbB4, E-cadherin, Bsg, EphA2, and Glut1, were decreased when the ESCs were cultured without LIF. Culturing in the absence of LIF also decreased the protein levels of the undifferentiated state-specific nuclear transcriptional factors, Oct-3/4 and Nanog. Under these conditions,

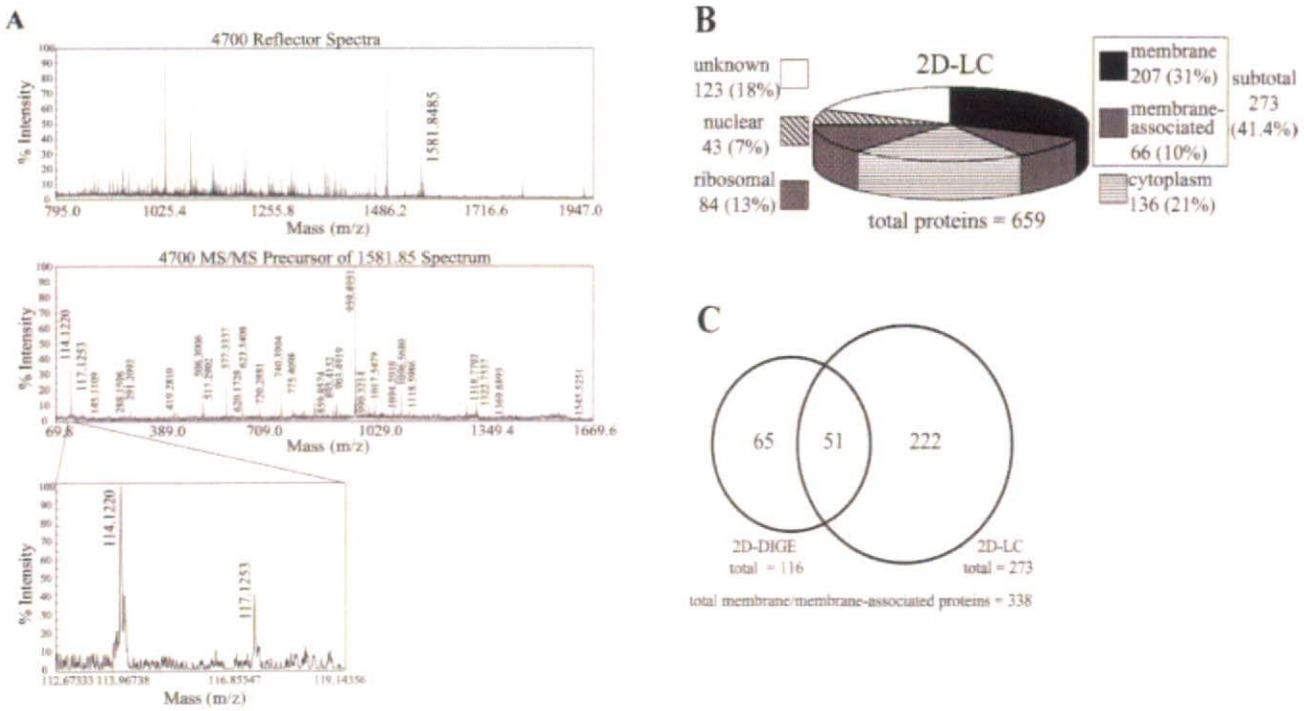

Figure 4. Shotgun-based analysis of membrane proteins of pluripotent and differentiated murine ESCs. (A) Examples of the MS and MS/MS spectra data obtained in the present study. The reporter peaks of m/z = 114 and 117 are from the iTRAQ reagents. The integration of the peak area reflects the quantity of peptide. (B) Subcellular localization of proteins identified using 2-D LC methods. (C) Venn diagram of shared and unique membrane and membrane-associated proteins identified by 2-D DIGE and 2-D LC. The numbers in the diagram indicate the number of identified proteins by each method.

the expression levels of a control protein, α-tubulin, were not decreased. The densitometric measurements of these bands from three independent experiments are summarized in Fig. 5B. Some of the identified proteins, *i.e.*, Slc16a1, Akt2, and ErbB4, were down-regulated to a greater extent than the well-established undifferentiated-state marker, Nanog. Immunofluorescence staining of murine ESCs cultured for 7 days without LIF further verified that the expression of these membrane proteins was specific for undifferentiated murine ESCs (Fig. 5C). Confocal microscopy of the undifferentiated murine ESCs revealed that Slc16a1 and Bsg colocalized to the surface of the plasma membrane in pluripotent murine ESCs (Fig. 5D), suggesting the cooperative action of these proteins in ESCs.

4 Discussion

Since undifferentiated murine ESCs are sensitive to extracellular stimuli, such as growth factors and extracellular matrix components, and can differentiate into various cell lineages, transmembrane and membrane-associated proteins are suggested to play important roles in the maintenance of pluripotency. In the present study, we prepared the membrane fractions from murine ESCs cultured with or without LIF for 7 days, *i.e.*, from pluripotent and differentiated cells, respectively. The observed profiles of undifferentiated cell markers (AP, Oct-3/4, and SSEA-1) and cell morphologies confirmed the successful preparation of cells used for subsequent proteomic analyses.

For the preparation of membrane fractions, two methods were used. For the 2-D DIGE analysis, the ESC surface proteins were labeled with a minimal concentration of impermeable biotinylating reagent. The membrane fractions were separated by sucrose density gradient centrifugation, and further purified using streptavidin beads. For the shotgun method, the plasma membrane fraction was prepared by sucrose density gradient centrifugation without biotinylation. Although the former method using biotin–avidin purification seems to be theoretically more effective than the latter method for the purification of membrane proteins, the results obtained from MS analyses of the former samples revealed that the percentage of membrane and membrane-associated proteins among the total identified proteins was at most 45%, while the latter method gave a similar percentage (41%). This could be due to the difficulties associated with the separation of hydrophobic proteins by IEF and SDS-PAGE. Similar results have been reported by other researchers using this method [14].

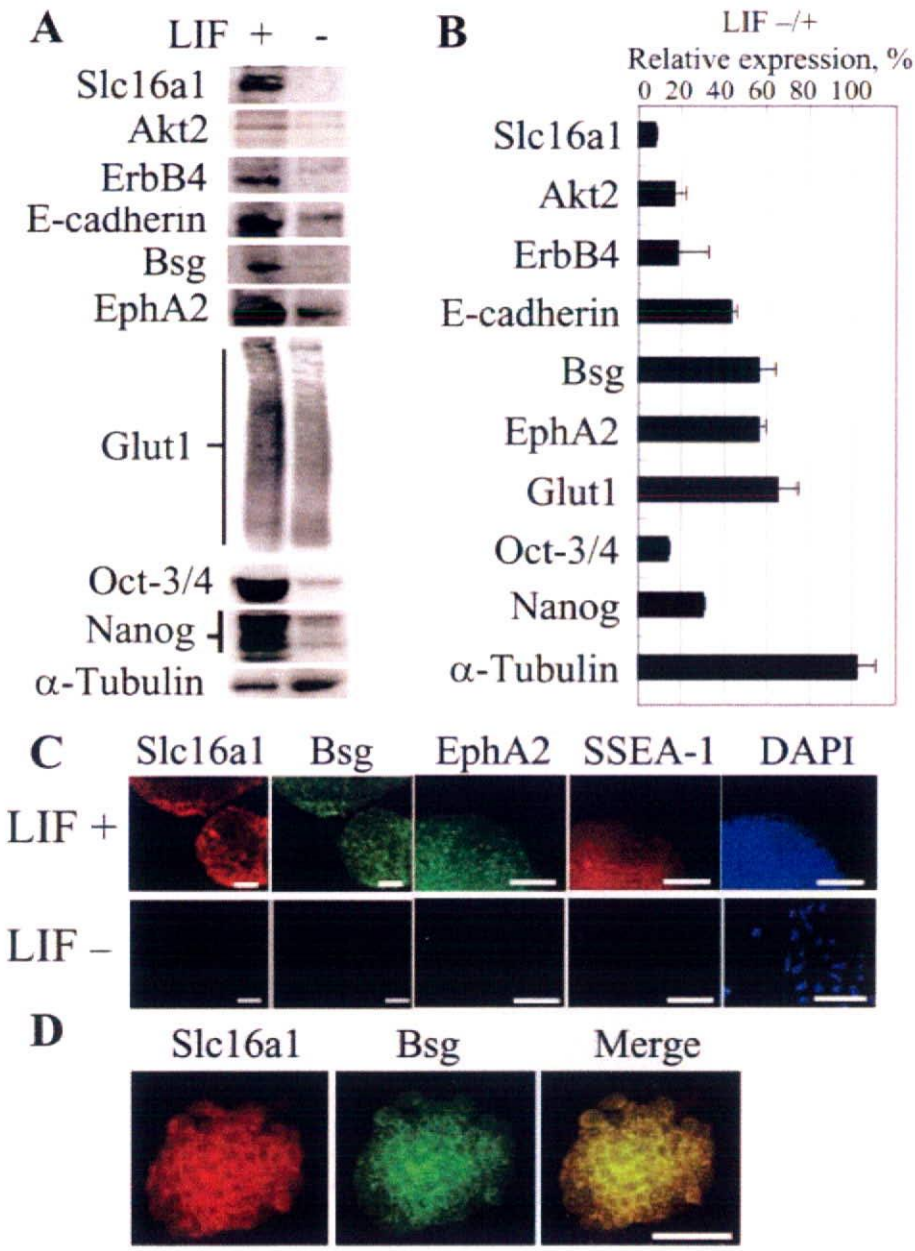

Figure 5. Undifferentiated state-specific membrane proteins expressed in murine ESCs. (A) Western blot analysis of pluripotent-specific membrane proteins in whole lysates of murine ESCs cultured for 7 days with or without LIF. The levels of these proteins were specifically decreased when the ESCs were cultured without LIF. (B) Quantification of the Western blotting in (A). The protein bands in the blots from three independent experiments were quantified using a densitometer. The amount of protein in the murine ESCs cultured with LIF was designated as 100. Error bars indicate the SEM of these experiments. The *p*-values calculated by Student's *t*-test were under 0.001. (C) Immunofluorescence analysis of the membrane proteins identified in murine ESCs. Bar, 200 μm. (D) Subcellular localization of Slc16a1 and Bsg in murine ESCs. Immunofluorescence analysis by confocal imaging reveals colocalization of Slc16a1 (red) and Bsg (green). Bar, 100 μm.

These problems can be overcome by using the shotgun method, in which membrane proteins are initially digested with a specific protease and the resultant small peptides are separated by multiple HPLCs. The shotgun method with 2-D LC gave apparently superior results to the 2-D gel-based method, and more than 80% of all the identified membrane and membrane-associated proteins were detected with this approach (Fig. 4C). Despite the disadvantage of hydrophobic membrane proteins, the 2-D gel-based method identified 33% of the total membrane and membrane-associated proteins (Fig. 4C). Moreover, the 2-D gel-based method identified 65 unique proteins that were not identified by the shotgun method. These results suggest that a complementary approach comprising the 2-D gel-based and shotgun-based methods would generate more complete lists of proteins, even when the samples were hydrophobic membrane proteins.

For the separation step of shotgun-based method, we adopted a ZIC-HILIC, with a combination of RPLC as the separation mode for the peptides after trypsin digestion. Recently, we compared this method with the most commonly used HPLC separation method, a combination of cation exchange chromatography with RPLC, using HSA as a model sample. ZIC-HILIC and RPLC gave superior separa-

Table 1. Examples of pluripotency-specific membrane proteins identified in the present study

GI accession no.	Protein identity	LIF ± ratio
gi|74183928	Solute carrier family 16 (monocarboxylic acid transporters), member 1	0.0000
gi|467233	Receptor-protein tyrosine kinase	0.1928
gi|23510249	WD repeat membrane protein PWDMP	0.2243
gi|26353502	Embigin	0.2360
gi|12836173	Solute carrier family 29 (nucleoside transporters), member 1	0.2498
gi|20072784	Thymoma viral proto-oncogene 2 (Akt2)	0.2562
gi|21730677	Chain C, alpha-catenin fragment, residues 385–651	0.2648
gi|74220144	Solute carrier organic anion transporter family, member 3a1	0.2803
gi|56748886	Sodium channel protein type 11 subunit alpha	0.2809
gi|13905180	Pyrroline-5-carboxylate reductase family, member 2	0.2901
gi|74355249	Olfactory receptor 424	0.2901
gi|94370659	Progesterone receptor membrane component 2	0.2929
gi|49750	Solute carrier family 3 (activators of dibasic and neutral amino acid transport) member 2	0.2932
gi|74215107	Solute carrier family 2 (facilitated glucose transporter), member 1	0.2963
gi|16307446	Bsg protein	0.3005
gi|11596855	Transferrin receptor	0.3105
gi|18044806	Glycoprotein, synaptic 2	0.3143
gi|83745122	Catenin (cadherin associated protein), delta 1	0.3165
gi|10946684	5-Hydroxytryptamine receptor 6	0.3249
gi|74195593	Solute carrier family 38, member 4	0.3400
gi|74198177	Integrin alpha 6	0.3434
gi|74141534	Solute carrier family 16 (monocarboxylic acid transporters), member 3	0.3438
gi|20070698	Solute carrier family 7, member 5	0.3608
gi|225753	E-cadherin	0.3618
gi|13876314	Protocadherin beta 6	0.3752
gi|94377177	Receptor-type tyrosine-protein phosphatase zeta precursor	0.3884
gi|10048460	Basal cell adhesion molecule	0.3989
gi|32057721	Olfactory receptor Olfr646	0.4383
gi|26364462	Bone marrow stromal cell antigen 2	0.4742
gi|21706627	Solute carrier family 2, member 3	0.4812
gi|22129197	Olfactory receptor 133	0.4873
gi|31560574	Integrin alpha 5	0.5086
gi|74184247	V-erb-a erythroblastic leukemia viral oncogene homolog 4	0.5128
gi|45504394	Integrin beta 1 (fibronectin receptor beta)	0.5163
gi|82659759	FAT tumor suppressor homolog 4	0.5714
gi|49903953	PTK7 protein tyrosine kinase 7	0.6286
gi|16307488	Interferon induced transmembrane protein 3	0.6712

tion of the peptide mixture and resulted in more MS/MS spectra of the peptides in the subsequent proteomic analysis (A. Intoh *et al.*, unpublished data). Our preliminary data from murine ESC membrane protein samples also suggests markedly improved protein identification with a combination of ZIC-HILIC and RPLC (data not shown).

After extensive database searching, the membrane and membrane-associated proteins specifically expressed in pluripotent murine ESCs were identified. They included receptors, channels, adhesion proteins, and signaling molecules. Among these, a pluripotent ESC-specific marker, E-cadherin, was identified. E-cadherin functions as an adhesion molecule during early embryonic development [26], and is used as a cell surface marker, as are SSEA-1 and AP activity, for ESCs [27]. We also identified β-catenin (see Supporting Information Table 2), which binds to E-cadherin [26]. Deletion of E-cadherin causes the differentiation of ESCs [28], which suggests important roles for E-cadherin in the maintenance of murine ESC pluripotency. The identification of these proteins verified the reliability of our quantitative proteomics analyses.

Some novel membrane proteins that are specifically expressed in pluripotent murine ESCs were identified. Solute carrier family 16, member 1 (Slc16a1) is one of the monocarboxylic acid transporter (Mct) family members. Bsg is a member of the Ig superfamily proteins and is a key factor in mouse blastocyst implantation [29]. Bsg interacts with Slc16a1 [29]. These two transmembrane proteins were down-regulated during the differentiation of murine ESCs (Figs. 5A–C). Colocalization of these proteins in murine

ESCs was confirmed by immunofluorescence analysis (Fig. 5D). Mct and Bsg function as essential transporters for pyruvate and lactate (but not glucose) as energy sources in very early embryogenesis [30]. Specific down-regulation of Slc16a1 and Bsg during the differentiation of murine ESCs suggests that these factors are also essential for the maintenance of the undifferentiated state of murine ESCs *in vitro*. Moreover, many solute carrier family members were identified as up- or down-regulated membrane proteins, which suggests dynamic switching of metabolite preferences during the differentiation of murine ESCs *in vitro* [31].

Another undifferentiated cell-specific protein, Akt2, is a member of the Rac serine/threonine protein kinase including Akt family, which is implicated in the regulation of cell cycle progression, cell death, adhesion, migration, metabolism, and tumorigenesis [32]. Phosphoinositide 3-kinase (PI3K)/Akt signaling has been proposed as a regulatory system for ESCs, and Akt1 is involved in the maintenance of murine and human ESCs [33]. After the withdrawal of LIF, the murine ESCs showed decreased expression of Akt2, which suggests that Akt2 plays similar functions to Akt1 in the maintenance of pluripotency. In addition, PI3K/Akt activated factors downstream of other signaling pathways, *e.g.*, basic FGF and integrins [34]. Thus, multiple signaling would cooperatively regulate the pluripotency of ESCs through activation of the PI3K/Akt signaling pathway. The increased expression of Akt2 in undifferentiated murine ESCs further underlines the importance of this protein for the maintenance of ESC multipotency.

EphA2 was also identified as a membrane protein that showed decreased expression during murine ESC differentiation upon LIF withdrawal. EphA2 is a member of the Eph family of receptor tyrosine kinases. Most Eph family members are expressed in developing embryos and tumor cells. The cellular function of EphA2 has been linked to cell proliferation [35]. The inhibition of EphA2 led to failure of growth and neoangiogenesis in human and mouse tumor cells [36]. Undifferentiated murine ESC-specific expression of EphA2 suggests the possibility that EphA2 plays similar roles in the proliferation of murine ESCs. Curiously, the expression of EphA2 is regulated by E-cadherin. Membrane localization and phosphorylation of EphA2 are dependent upon E-cadherin-mediated adhesion in mammary epithelial cells [37]. Moreover, deletion of E-cadherin leads to failure of the EphA2 receptor to localize at cell–cell contact points [38]. Cooperative down-regulation of EphA2 and E-cadherin during murine ESC differentiation may contribute to the efficient dissociation of murine ESCs from the round-shaped colonies and may promote differentiation by modulating cell proliferation.

Proteomic analysis with 2-D DIGE also identified the epidermal growth factor receptor family member ErbB4 as one of the membrane proteins down-regulated during murine ESC differentiation. ErbB4 is expressed in developing and mature organs, including the heart, breast, and brain [39]. The ErbB receptors (ErbB1–4) and their ligands, neuregulins, function cooperatively for the survival and proliferation of skeletal muscle stem cells [40]. Gene-targeted inactivation of ErbB4 in mice results in mid-embryonic lethality due to failure of myocardial trabeculae development [39]. Moreover, neuregulins promote the proliferation of hippocampus-derived neural progenitor cells (NPCs) and maintain the progenitor states of NPCs *via* the ErbB-phospholipase C/protein kinase C (PLC/PKC) pathway [41]. Thus, ErbB4 appears to be an essential factor for embryogenesis and the proliferation of stem cells. Our finding of pluripotent murine ESC-specific expression of ErbB4 suggests an additional function as a factor promoting the proliferation of murine ESCs.

In conclusion, this is the first report of the quantitative proteomics of the membrane proteins in pluripotent and differentiated ESCs. We hypothesized that pluripotent stem cells have functional and specific surface membrane proteins given their sensitivity to extracellular conditions. Indeed, various receptors and cell adhesion molecules that are specifically expressed in pluripotent murine ESCs were successfully identified, suggesting that these ligand-receptor signaling activities are crucial for murine ESC pluripotency. Moreover, other pluripotency-specific membrane proteins, such as transporters and channels, were identified. These results suggest that the transport of small molecules across the plasma membrane regulates the pluripotency of murine ESCs. These membrane proteins identified in pluripotent murine ESCs may be useful as pluripotency-specific markers or surface antigens for stem cell purification. These membrane proteins may be involved not only in the maintenance of pluripotency, but also in the reprogramming of somatic cells, as described recently [42, 43], whereby a combination of ESC-specific factors reprograms embryonic and somatic fibroblasts to induce pluripotent stem (iPS) cells. Further investigations will uncover the precise roles of these identified membrane proteins in the regulation of ESCs.

We are grateful to Chizuko Takamura for excellent technical assistance with the MALDI-TOF-MS/MS analysis.

The authors have declared no conflict of interest.

5 References

[1] Evans, M. J., Kaufman, M. H., Establishment in culture of pluripotential cells from mouse embryos. *Nature* 1981, *292*, 154–156.

[2] Martin, G. R., Isolation of a pluripotent cell line from early mouse embryos cultured in medium conditioned by teratocarcinoma stem cells. *Proc. Natl. Acad. Sci. USA* 1981, *78*, 7634–7638.

[3] Bradley, A., Evans, M., Kaufman, M. H., Robertson, E., Formation of germ-line chimaeras from embryo-derived teratocarcinoma cell lines. *Nature* 1984, *309*, 255–256.

[4] Donovan, P. J., Gearhart, J., The end of the beginning for pluripotent stem cells. *Nature* 2001, *414*, 92–97.

[5] Prelle, K., Zink, N., Wolf, E., Pluripotent stem cells–model of embryonic development, tool for gene targeting, and basis of cell therapy. *Anat. Histol. Embryol.* 2002, *31*, 169–186.

[6] Smith, A. G., Heath, J. K., Donaldson, D. D., Wong, G. G. *et al.*, Inhibition of pluripotential embryonic stem cell differentiation by purified polypeptides. *Nature* 1988, *336*, 688–690.

[7] Williams, R. L., Hilton, D. J., Pease, S., Willson, T. A. *et al.*, Myeloid leukaemia inhibitory factor maintains the developmental potential of embryonic stem cells. *Nature* 1988, *336*, 684–687.

[8] Nunomura, K., Nagano, K., Itagaki, C., Taoka, M. *et al.*, Cell surface labeling and mass spectrometry reveal diversity of cell surface markers and signaling molecules expressed in undifferentiated mouse embryonic stem cells. *Mol. Cell. Proteomics* 2005, *4*, 1968–1976.

[9] Baharvand, H., Fathi, A., van Hoof, D., Salekdeh, G. H., Concise review: Trends in stem cell proteomics. *Stem Cells* 2007, *25*, 1888–1903.

[10] Yamanaka, S., Li, J., Kania, G., Elliott, S. *et al.*, Pluripotency of embryonic stem cells. *Cell Tissue Res.* 2008, *331*, 5–22.

[11] Boiani, M., Scholer, H. R., Regulatory networks in embryo-derived pluripotent stem cells. *Nat. Rev. Mol. Cell Biol.* 2005, *6*, 872–884.

[12] Wallin, E., von Heijne, G., Genome-wide analysis of integral membrane proteins from eubacterial, archaean, and eukaryotic organisms. *Protein Sci.* 1998, *7*, 1029–1038.

[13] Hopkins, A. L., Groom, C. R., The druggable genome. *Nat. Rev. Drug Discov.* 2002, *1*, 727–730.

[14] Klein, C., Garcia-Rizo, C., Bisle, B., Scheffer, B. *et al.*, The membrane proteome of *Halobacterium salinarum*. *Proteomics* 2005, *5*, 180–197.

[15] Santoni, V., Kieffer, S., Desclaux, D., Masson, F., Rabilloud, T., Membrane proteomics: Use of additive main effects with multiplicative interaction model to classify plasma membrane proteins according to their solubility and electrophoretic properties. *Electrophoresis* 2000, *21*, 3329–3344.

[16] Unlu, M., Morgan, M. E., Minden, J. S., Difference gel electrophoresis: A single gel method for detecting changes in protein extracts. *Electrophoresis* 1997, *18*, 2071–2077.

[17] Wu, C. C., Yates, J. R., III, The application of mass spectrometry to membrane proteomics. *Nat. Biotechnol.* 2003, *21*, 262–267.

[18] Nagele, E., Vollmer, M., Horth, P., Vad, C., 2D-LC/MS techniques for the identification of proteins in highly complex mixtures. *Expert Rev. Proteomics* 2004, *1*, 37–46.

[19] Wu, W. W., Wang, G., Baek, S. J., Shen, R. F., Comparative study of three proteomic quantitative methods, DIGE, cICAT, and iTRAQ, using 2D gel- or LC-MALDI TOF/TOF. *J. Proteome Res.* 2006, *5*, 651–658.

[20] Ross, P. L., Huang, Y. N., Marchese, J. N., Williamson, B. *et al.*, Multiplexed protein quantitation in *Saccharomyces cerevisiae* using amine-reactive isobaric tagging reagents. *Mol. Cell. Proteomics* 2004, *3*, 1154–1169.

[21] Gygi, S. P., Rist, B., Gerber, S. A., Turecek, F. *et al.*, Quantitative analysis of complex protein mixtures using isotope-coded affinity tags. *Nat. Biotechnol.* 1999, *17*, 994–999.

[22] Zhao, Y., Zhang, W., White, M. A., Zhao, Y., Capillary high-performance liquid chromatography/mass spectrometric analysis of proteins from affinity-purified plasma membrane. *Anal. Chem.* 2003, *75*, 3751–3757.

[23] Iwafune, Y., Kawasaki, H., Hirano, H., Electrophoretic analysis of phosphorylation of the yeast 20S proteasome. *Electrophoresis* 2002, *23*, 329–338.

[24] Wobus, A. M., Holzhausen, H., Jakel, P., Schoneich, J., Characterization of a pluripotent stem cell line derived from a mouse embryo. *Exp. Cell Res.* 1984, *152*, 212–219.

[25] Matsui, Y., Zsebo, K., Hogan, B. L., Derivation of pluripotential embryonic stem cells from murine primordial germ cells in culture. *Cell* 1992, *70*, 841–847.

[26] Butz, S., Larue, L., Expression of catenins during mouse embryonic development and in adult tissues. *Cell Adhes. Commun.* 1995, *3*, 337–352.

[27] Viswanathan, S., Benatar, T., Rose-John, S., Lauffenburger, D. A., Zandstra, P. W., Ligand/receptor signaling threshold (LIST) model accounts for gp130-mediated embryonic stem cell self-renewal responses to LIF and HIL-6. *Stem Cells* 2002, *20*, 119–138.

[28] Larue, L., Antos, C., Butz, S., Huber, O. *et al.*, A role for cadherins in tissue formation. *Development* 1996, *122*, 3185–3194.

[29] Iacono, K. T., Brown, A. L., Greene, M. I., Saouaf, S. J., CD147 immunoglobulin superfamily receptor function and role in pathology. *Exp. Mol. Pathol.* 2007, *83*, 283–295.

[30] Herubel, F., El Mouatassim, S., Guerin, P., Frydman, R., Menezo, Y., Genetic expression of monocarboxylate transporters during human and murine oocyte maturation and early embryonic development. *Zygote* 2002, *10*, 175–181.

[31] Leese, H. J., Barton, A. M., Pyruvate and glucose uptake by mouse ova and preimplantation embryos. *J. Reprod. Fertil.* 1984, *72*, 9–13.

[32] Brazil, D. P., Yang, Z. Z., Hemmings, B. A., Advances in protein kinase B signalling: AKTion on multiple fronts. *Trends Biochem. Sci.* 2004, *29*, 233–242.

[33] Dreesen, O., Brivanlou, A. H., Signaling pathways in cancer and embryonic stem cells. *Stem Cell Rev.* 2007, *3*, 7–17.

[34] Xu, R. H., Peck, R. M., Li, D. S., Feng, X. *et al.*, Basic FGF and suppression of BMP signaling sustain undifferentiated proliferation of human ES cells. *Nat. Methods* 2005, *2*, 185–190.

[35] Fang, W. B., Brantley-Sieders, D. M., Parker, M. A., Reith, A. D., Chen, J., A kinase-dependent role for EphA2 receptor in promoting tumor growth and metastasis. *Oncogene* 2005, *24*, 7859–7868.

[36] Vearing, C. J., Lackmann, M., "Eph receptor signalling; dimerisation just isn't enough". *Growth Factors* 2005, *23*, 67–76.

[37] Zantek, N. D., Azimi, M., Fedor-Chaiken, M., Wang, B. *et al.*, E-cadherin regulates the function of the EphA2 receptor tyrosine kinase. *Cell Growth Differ.* 1999, *10*, 629–638.

[38] Orsulic, S., Kemler, R., Expression of Eph receptors and ephrins is differentially regulated by E-cadherin. *J. Cell Sci.* 2000, *113*, 1793–1802.

[39] Jones, F. E., Golding, J. P., Gassmann, M., ErbB4 signaling during breast and neural development: Novel genetic models reveal unique ErbB4 activities. *Cell Cycle* 2003, *2*, 555–559.

[40] Golding, J. P., Calderbank, E., Partridge, T. A., Beauchamp, J. R., Skeletal muscle stem cells express anti-apoptotic ErbB receptors during activation from quiescence. *Exp. Cell Res.* 2007, *313*, 341–356.

[41] Edwards, J. M., Bottenstein, J. E., Neuregulin 1 growth factors regulate proliferation but not apoptosis of a CNS neuronal progenitor cell line. *Brain Res.* 2006, *1108*, 63–75.

[42] Takahashi, K., Yamanaka, S., Induction of pluripotent stem cells from mouse embryonic and adult fibroblast cultures by defined factors. *Cell* 2006, *126*, 663–676.

[43] Takahashi, K., Tanabe, K., Ohnuki, M., Narita, M. *et al.*, Induction of pluripotent stem cells from adult human fibroblasts by defined factors. *Cell* 2007, *131*, 861–872.

Journal of Bioscience and Bioengineering
VOL. 107 No. 1, 95–97, 2009

ELSEVIER

www.elsevier.com/locate/jbiosc

TECHNICAL NOTE

Mutagenesis of longer inserts by the ligation of two PCR fragments amplified with a mutation primer

Yu Kato, Noriaki Arakawa, Yusuke Masuishi, Hiroshi Kawasaki,* and Hisashi Hirano

Supramolecular Biology, International Graduate School of Arts and Sciences, Yokohama City University, Suehiro-cho 1-7-29, Tsurumi-ku, Yokohama 230-0045, Japan

Received 11 July 2008; accepted 11 September 2008

We report a method for efficient mutagenesis of DNA in large vectors without subcloning. Two segments of the target DNA sequence, one having a mutation introduced via a mutant primer, were amplified by PCR and then the purified fragments were ligated to a vector. The mutation efficiency was nearly 100%.

[**Key words:** Polymerase chain reaction (PCR); Mutagenesis; Yeast; Expression vector; Deletion; Insertion; Substitution]

Techniques for site-directed mutagenesis have been widely used to analyze the function and regulation of genes (1–3) and the various PCR-based mutagenetic methods have improved each year (4). Among them, inverse PCR-based mutagenesis using tools such as the QuikChange® Site-Directed Mutagenesis Kit (Stratagene, La Jolla, CA, USA) is widely used (5, 6). Although this method is relatively efficient for small-size vectors (up to approximately 4000 bp), the efficiency greatly decreases as the target size increases. Additionally, for efficient mutation, the necessary length of the two complementary synthetic primers is 30–45 mer (usually longer than 40 mer). Another choice is the megaprimer method (7, 8). Although this method is applicable to large-size vectors, its lower efficiency makes it necessary to subclone the PCR product and confirm its sequence. To circumvent these problems, we report a reliable method of mutagenesis of DNA in a large-size vector (Fig. 1). We applied the method of Kadowaki et al. (9) to the mutagenesis of long inserts in a large-size vector. The method introduces mutations in DNA by ligating two fragments of the target region, one of which is amplified with a mutagenic primer by PCR. Both segments are amplified with vector-derived primers outside of the multiple-cloning site, such as a T7 promoter or T7 terminator. This PCR design makes ligation to vectors at similar cloning sites possible following digestion with restriction enzymes. Since this method amplifies only the inserts by PCR, unlike inverse PCR, mutagenesis of the targets cloned in a large-size vector such as expression vectors for yeast cells. PCR reaction used in the method is the same as routine amplification, which reduces unexpected errors. By replacing *Taq* polymerase with a high fidelity thermostable DNA polymerase with proofreading, more reliable amplification for the longer fragments to mutagenesis became possible without blunt-end treatment. The PCR products amplified by the DNA polymerase with 3′ to 5′ exonuclease activity are blunt-ended, which enables the ligation of two PCR segments without the insertion or deletion of bases, after restriction enzyme digestion at vector derived sites. Each of two purified PCR segments is successively ligated to a vector in one tube. This simple method is applicable to an insert in a large-size plasmid (e.g., cell line/yeast expression vectors) with relatively short primers (about a 20-mer). Primer design for mutagenesis is as simple as conventional PCR amplification. The PCR products could be cloned directly in the relatively large plasmid, such as pGL3-basic (4818 bp, Promega, Madison, WI, USA) and pRS425 (6849 bp, (10)), without subcloning (Table 1).

The detailed procedures to make an *Mlu*I cleavable site (5′-ACGCGT-3′) just downstream of the start codon of yeast *BUD8* (11) are as follows: the plasmid pYC14 (cloned with pRS425 vector, total size of 9987 bp), carrying upstream 808 bp, an open reading frame of *BUD8*, and downstream 517 bp, was used to insert an *Mlu*I restriction site (5′-ACGCGT-3′) just downstream of the start codon of the open reading frame. PCR was performed in two separate tubes using the corresponding sets of primer pairs, T7 promoter forward primer, 5′-TAATA CGACT CACTA TAGGG-3′ (20-mer)/BUD8_R 5′-CATAC TTCAT GTAGA ATCG-3′ (19-mer) or BUD8_F 5′-**ACGCG T** (*Mlu*I) ATAC AATCA GACGA AG-3′ (22-mer)/M13 reverse primer 5′-CAGGA AACAG CTATG AC-3′ (17-mer). The 50-μL reaction mixture contained 10× KOD-plus-buffer, 0.2 mM dNTP, 1 mM $MgSO_4$, 1–2 ng of the template plasmid (pYC14), 2 μM of each primer, and 1 unit of the proof-reading thermostable DNA polymerase, KOD-plus-DNA polymerase (Toyobo, Osaka). The mixture was initially run at 96 °C for 2 min, and then for 30 cycles of PCR. Each cycle consisted of denaturation at 94 °C for 15 s, annealing at 55 °C for 15 s, and extension at 68 °C for 2.5 min. The last extension step was performed at 68 °C for 7 min. After agarose-gel purification of the PCR products, one PCR fragment was digested with SpeI to remove 43 bp fragments at upstream end and the other with

* Corresponding author. Tel.: +81 045 508 7556; fax: +81 045 508 7667.
E-mail address: kawasaki@yokohama-cu.ac.jp (H. Kawasaki).

1389-1723/$ - see front matter © 2008, The Society for Biotechnology, Japan. All rights reserved.
doi:10.1016/j.jbiosc.2008.09.003

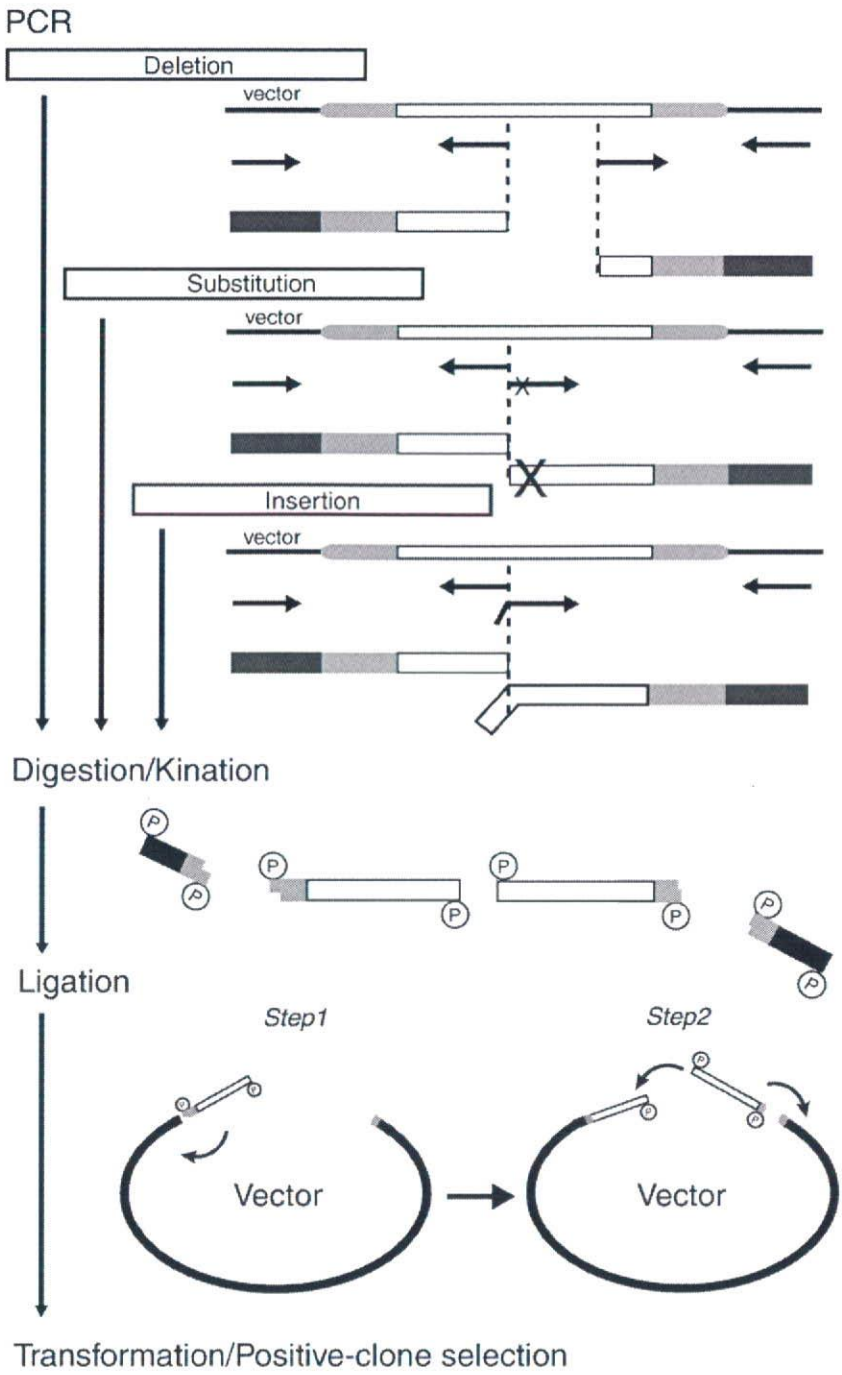

FIG. 1. Schematic illustration of the procedures used for insertion, substitution, and deletion. The forward primer for one segment and reverse primer for the other segment were vector-derived (T7 promoter and T7 terminator). The mutation was added in the specific primer to the gene of interest (GOI). Any plasmid in which the GOI was inserted could be used as a template. The black, gray, and white boxes show the backbone, multiple-cloning site, and GOI, respectively. The terminus of the PCR product near the mutation is blunt and phosphorylated, whereas the other terminus has an overhang digested with a restriction enzyme, which makes ligation to multiple vector cloning sites possible. One fragment and the predigested vector were ligated with a ligation mix for a short period, and then the other fragment was added to the same tube. The mutation was confirmed by colony PCR, restriction enzyme mapping, and sequence analysis.

*Xho*I to remove 101 bp fragments at downstream end, and the fragments were simultaneously phosphorylated with T4 polynucleotide kinase (Takara Bio, Otsu, Japan). The resulting *Spe*I and *Xho*I fragments were then purified with the Wizard® SV Gel and PCR Clean-Up System (Promega), which can remove fragments of less than 100 bp. The fragments were recovered in 20 μL of DNase-free water. The ligation of the fragments to the vector was performed by a two-step procedure: the 2.5 μL of SpeI fragments and *Spe*I/*Xho*I-digested pRS425 were incubated with 5.5 μL of ligation mix (Takara Bio) for 30 min at 16 °C in a tube. The 2.5 μL of *Xho*I fragments were then added to the same tube. The ligation reaction continued for 1 h at 16 °C. The vector, ligated with an insert DNA, was transformed to competent cells of *Escherichia coli*, XL10 Gold strain. Colony PCR was performed by using vector-derived primers, the T7 promoter primer, TAATA CGACT CACTA TAGGG (20-mer), and the M13-R primer, GGAAA CAGCT ATGAC CATGA (20-mer), generating approximately 3500-bp

TABLE 1

Mutagenesis	Vector[a]	Vector size (bp)	Insert size (bp)	Insert check[b,c]	Sequencing[d]
Deletion	pGL3-basic	4818	607[f]	5 (8)	5
Insertion	pRS425	6849	3138[g]	3 (48)[e]	3
	pRS426	5726	3245[h]	8 (48)[e]	8
	pRS305	5504	1698[i]	7 (10)	7
Substitution	pBluescript (SK−)	2961	2832[j]	8 (20)	7

[a] pRS425 pRS426 and pRS305, see Ref (10, 12). pBluescript (SK−) and pGL3-basic vectors were purchased from Stratagene and Promega, respectively.

[b] The number of colony carrying a vector with an insert is shown. The number of colony analyzed by colony PCR is shown in parentheses.

[c] Colony PCR was performed by following condition; the 10-μL reaction mixture contained 10× *Ex Taq* buffer, 0.2 mM dNTP, 2 μM of each primer, and 0.1 unit of *TaKaRa Ex Taq*™ DNA polymerase (Takara Bio). The mixture was initially run at 94 °C for 5 min, and then for 35 cycles of PCR. Each cycle consisted of denaturation at 94 °C for 30 s, annealing at 55 °C for 1 min, and extension at 72 °C for 4 min. The last extension step was performed at 72 °C for 7 min.

[d] Sequencing analysis of the inserts, which were positive by colony PCR, was carried out to confirm the mutation. The number of inserts with correct mutation is shown.

[e] Since we performed colony PCR to generate 3500-bp bands as a first-insert check screen, some colonies carrying the vector with insert were dropped by failed PCR reactions.

[f] *ANX4* at position 39801481–39802065 in chromosome II of *Homo sapiens* (NCBI accession no. NW_001838769.1).

[g] *BUD8* at position 4086–7223 in chromosome XII of *Saccharomyces cerevisiae* (NCBI accession no. U19102).

[h] *BUD9* at position 1778–3245 in chromosome VII of *Saccharomyces cerevisiae* (NCBI accession no. DQ 115391).

[i] *CGI121* at position 5575–7668 in chromosome XIII of *Saccharomyces cerevisiae* (NCBI accession no. Y07777).

[j] *BUD32* at position 205090–206869 in chromosome VII of *Saccharomyces cerevisiae* (NCBI accession no. NC_001145).

bands. The plasmids extracted from the colonies were digested with *SpeI*/*XhoI* to confirm whether they had the correct inserts. The plasmids were also subjected to sequence analysis. In this case, all colonies with an insert carried a plasmid with the insertion of the *MluI* restriction site. We also performed deletion experiments by using the pGL3-basic vector, and substitution experiments by using pBluescript (SK−) vector (Table 1).

The efficiency of mutagenesis by this method using various vectors and inserts is summarized in Table 1. In the case of random colony pickup, about 10–60% of colonies carried a vector with an insert. Sequence analysis of the inserts revealed that the mutation desired was successfully introduced into nearly 100% in the vector with an insert (Table 1). The efficiency of three-piece ligation is not high enough for longer inserts, so the ratio of colonies carrying an empty vector is a little high in some cases. In conclusion, this method for the large vectors is a very powerful tool for insertion, substitution, and deletions of base pairs in DNA.

References

1. **Ling, M. M. and Robinson, B. H.:** Approaches to DNA mutagenesis: an overview, Anal. Biochem., **254**, 157–178 (1997).
2. **Miyashita, M., Shugyo, M., and Nikawa, J. I.:** Mutational analysis and localization of the inositol transporters of *Saccharomyces cerevisiae*, J. Biosci. Bioeng., **96**, 291–297 (2003).
3. **Hosomi, N., Kawamura-Konishi, Y., Kawano, R., Fujii, I., and Suzuki, H.:** Site-directed mutagenesis study of the antibody 2D7 which catalyzes a reaction for insertion of Cu^{2+} into mesoporphyrin, J. Biosci. Bioeng., **99**, 222–229 (2005).
4. **Li, M. Z. and Elledge, S. J.:** Harnessing homologous recombination *in vitro* to generate recombinant DNA via SLIC, Nature, **4**, 251–256 (2007).
5. **Imai, Y., Matsushima, T., Sugimura, M., and Terada, A.:** simple and rapid method for generating a deletion by PCR, Nucleic Acids Res., **19**, 2785 (1991).
6. **Li, J., Li, C., Xiao, W., Yuan, D., Wan, G., and Ma, L.:** Site-directed mutagenesis by combination of homologous recombination and *Dpn*I digestion of the plasmid template in *Escherichia coli*, Anal. Biochem., **373**, 389–391 (2008).
7. **Nabavi, S. and Nazar, R. N.:** Simplified one-tube "megaprimer" polymerase chain reaction mutagenesis, Anal. Biochem., **345**, 346–348 (2005).
8. **Chapnik, N., Sherman, H., and Froy, O.:** A one-tube site-directed mutagenesis method using PCR and primer extension., Anal. Biochem., **372**, 255–257 (2008).
9. **Kadowaki, H., Kadowaki, T., Wondisford, F. E., and Taylar, S. I.:** Use of polymerase chain reacrion catalyzed by *Taq* DNA polymerase for site-specific mutagenesis, Gene, **76**, 161–166 (1989).
10. **Christianson, T. W., Sikorski, R. S., Dante, M., Shero, J. H., and Hieter, P.:** Multifunctional yeast high-copy-number shuttle vectors, Gene, **110**, 119–122 (1992).
11. **Zahner, J. E., Harkins, H. A., and Pringle, J. R.:** Genetic analysis of the bipolar pattern of bud site selection in the yeast *Saccharomyces cerevisiae*, Mol. Cell. Biol., **16**, 1857–1870 (1996).
12. **Sikorski, R. S. and Hieter, P.:** A system of shuttle vectors and yeast host strains designed for efficient manipulation of DNA in *Saccharomyces cerevisiae*, Genetics, **122**, 19–27 (1989).

Hiroshi Kawasaki
Akiko Okayama
Yuko Iwafune
Shota Yahagi
Noriaki Arakawa
Hisashi Hirano

Supramolecular Biology, International Graduate School of Arts and Sciences, Yokohama City University, Yokohama, Japan

Received March 26, 2008
Revised June 6, 2008
Accepted June 20, 2008

Short Communication

Multiplex detection and identification of proteins on a PVDF membrane blocked with a synthetic polymer-based reagent

2-DE is one of the most powerful methods for analyzing proteins expressed in cells and tissues. Immunodetection of proteins blotted on a polymer membrane is the method of choice for detecting specific proteins in 2-D gels. To precisely locate spots of immunoreactive proteins in 2-D gels, both dye staining and immunodetection were performed on the same PVDF membrane. Prior to immunodetection, nonspecific adsorption of the antibodies to the membrane was blocked with a synthetic polymer-based reagent (N-102) after protein transfer. The protein was then stained with colloidal gold or CBB followed by protein spot identification by LC-MS. Described herein is a method for multiplex analysis of proteins transferred to a PVDF membrane. Proteins that were phosphorylated at tyrosine in the phosphoproteome of rice callus or human ovarian cancer cells were detected by immunoblotting and subsequently identified with high precision.

Keywords:
Immunodetection / Mass spectrometry / PVDF membrane
DOI 10.1002/elps.200800200

2DE is one of the most powerful methods used to analyze proteins expressed in cells and tissues [1]. Proteins separated by electrophoresis are typically detected by staining with traditional dyes such as CBB [2], and SYPRO Ruby or Flamingo [3]. Immunodetection is typically performed after transferring the proteins onto a polymer membrane [4]. This is the method of choice for the detection of specific proteins in 2-D gels. Of the thousands of proteins separated in dye-stained 2-D gels, only a few are typically observed after immunodetection. Identification of immunoreactive proteins in the constellation of protein spots in 2-DE requires a side-by-side comparison of two membranes, a blot in which the total protein content is stained with a nonspecific dye and an immunoblot stained with a specific antibody. This is sometimes difficult, since protein separation performed in two separate gels is not identical. To avoid these complications and precisely locate immunoreactive proteins in 2-D gels, nonspecific staining and immunodetection must be carried out on the same membrane. Several methods have reported visualization of total protein before and after immunodetection. For example, reversible staining of blots with Ponceau S has been widely applied before immunodetection [5]. It, however, is not sufficiently sensitive to detect proteins separated by 2-D PAGE, and is used primarily to locate immunoreactive proteins or to confirm protein transfer. SYPRO Rose Plus, a europium-based metal chelate protein stain, is sensitive, reversible [6], and compatible with immunodetection. Staining with colloidal gold after immunodetection has also been reported [7–9], and has exhibited sufficient sensitivity to locate spots of immunoreactive protein. Ducret *et al.* reported that subjecting PVDF membranes to a PVP-40 treatment prior to immunodetection *via* chemiluminescence was compatible with the visualization of total protein provided by colloidal gold staining. Duong and Chang reported that a nitrocellulose membrane, blocked with nonfat dry milk prior to staining with 5-bromo-4-chloro-3-indolyl phosphate/nitro blue tetrazone, could be counterstained with colloidal gold after air-drying overnight at room temperature.

Immunodetection utilizing specific antibodies can succinctly identify a protein in an electrophoresis spot. However, the proteins detected with group-specific antibodies such as phosphotyrosine or oxidized protein-specific antibodies require further identification. Protein spot identification by MS has become widely used in conjunction with in-gel or on-membrane digestion [10]. The method is sufficiently sensitive to identify proteins in spots at femtomole quantities.

Phosphorylation is an important modification of proteins that serves to regulate a wide range of biological processes such as the cell cycle and cell death by modulating the signal transduction mechanism of the kinase cascade. Phosphorylation of proteins occurs mainly at serine and threonine, but may also occur at tyrosine. Some tyrosine kinases were originally discovered as products of oncogenes, and have critical roles in the oncogenic process. It has become evident, however, that tyrosine phosphorylation controls a much wider range of

Correspondence: Dr. Hiroshi Kawasaki, Yokohama City University, Suehiro-cho 107-29, Tsurumi-ku, Yokohama 230-0045, Japan
E-mail: kawasaki@yokohama_cu.ac.jp
Fax: +81-45-508-7667

Abbreviation: TBST, TBS with Tween 20

biological processes. In plants, no classical protein tyrosine kinases have been identified in the genome. Recent studies [11] have revealed that plants lack a bona fide tyrosine kinase and that tyrosine phosphorylation is carried out by dual-specificity STY kinases. This work describes an analysis of the phosphoproteome of rice callus and ovarian cancer cells to identify proteins that were phosphorylated at tyrosine using 2-D PAGE and phosphotyrosine-specific antibodies. Multiplex analyses of proteins transferred to a PVDF membrane were performed using a nonprotein blocking reagent. This method thereby enabled immunodetection, total protein detection, and protein identification with MS on the same membrane. The blocking reagent N-102 (NOF Corporation) is a synthetic polymer-based reagent that was developed for blocking nonspecific adsorption in immunoassay plates. The structure or composition of N-102 is not open to the public. It is a hydrophilic polymer with molecular-weight distribution around hundreds of kDa, though. The presence of N-102 on a PVDF membrane after protein transfer was compatible with immunodetection and allowed for subsequent protein staining with colloidal gold or CBB and protein spot identification by LC-MS.

Rice callus was induced from seeds on agar containing Murashige–Skoog medium. Proteins were extracted by grinding the callus with a mortar and pestle in lysis buffer (8 M urea, 2 M thiourea, 3% CHAPS, 1% NP-40, 2% ampholine, 5% 2-mercaptoethanol, and 5% PVP). The mixture was centrifuged and the resulting supernatant was recovered. Polyphenol and lipid components were removed by hexane extraction. Approximately 5 μg of protein was separated by 2-D PAGE. The first dimension consisted of 3–10 NL (11 cm, Bio-Rad); the second dimension consisted of SDS-PAGE with 12% polyacrylamide gel *via* the Laemmli method. Figure 1A shows a typical result of 2-D PAGE performed on rice proteins visualized by colloidal gold (Bio-Rad) staining after transfer to a PVDF membrane (Immobilon-P; Millipore). The membrane was washed twice for 20 min with TBS with Tween 20 (TBST) (0.05% Tween 20, 20 mM Tris–HCl (pH 7.5), and 0.15 M NaCl) and again with five repetitions of water for 2 min each. The membrane was then stained with colloidal gold without the use of any N-102 blocking reagent.

Proteins phosphorylated at tyrosine were detected with mouse monoclonal antibodies specific to phosphotyrosine (P-Tyr-100; Cell Signaling Technology). After transferring the proteins to the PVDF membrane, the membrane was washed twice for 5 min with TBST and soaked for 60 min in a solution of N-102, diluted by one-fifth with TBST. The membrane was once again rinsed twice with TBST for 5 min and incubated overnight in a solution of P-Tyr-100 antibodies (1/2000 in TBST) at 4°C. Finally, the membrane was again rinsed twice with TBST for 5 min and incubated with a secondary antibody solution (horse radish peroxidase-labeled rabbit antibody

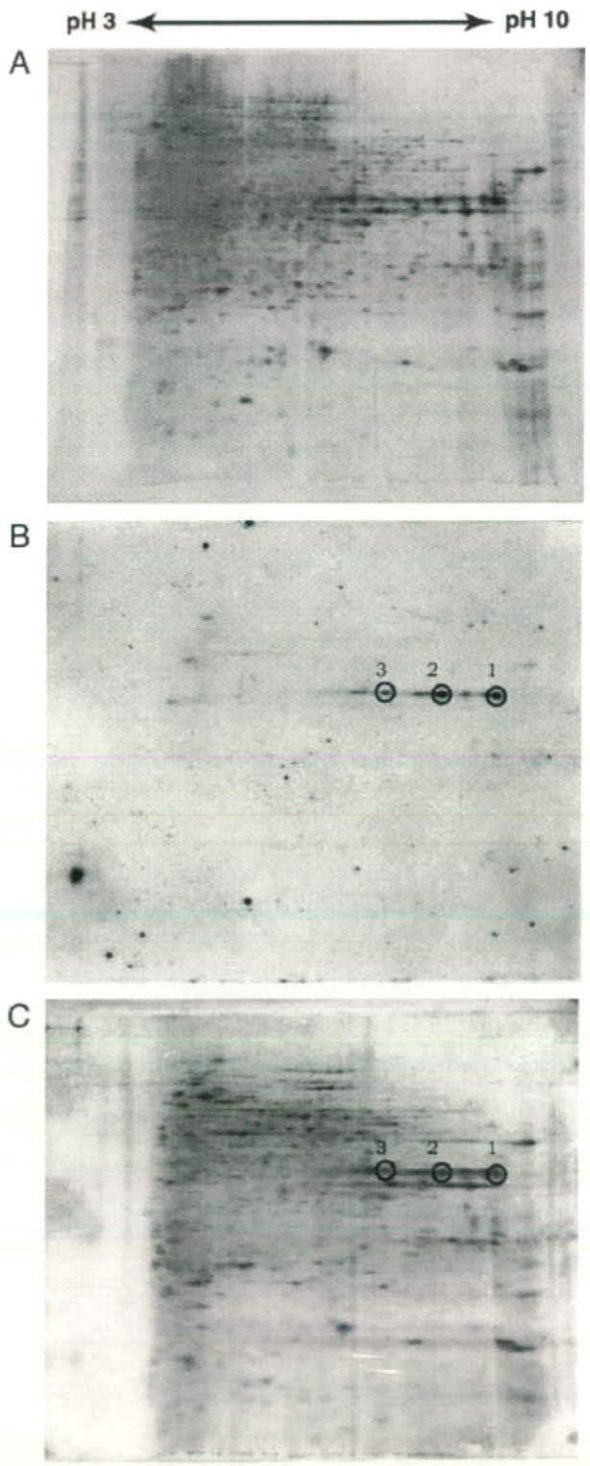

Figure 1. Rice callus proteins were separated by 2-D PAGE and transferred to a PVDF membrane. (A) Proteins were stained with colloidal gold in the absence of N-102 blocking reagent. (B) Phosphorylated proteins were detected by immunodetection using phosphotyrosine-specific antibody (P-Tyr-100). Nonspecific adsorption of antibodies to the PVDF membrane was blocked with N-102, and the detection was performed by ECL. (C) The same membrane in B was stained with colloidal gold. Spots 1–3 in C were subjected to subsequent MS analyses to identify the proteins. Fructose-bisphosphate aldolase (ALF_ORYSJ) was identified in each spot by MS/MS ion search of Mascot (database: SwissProt 54.6 ×, taxonomy: Oryza sativa, enzyme: trypsin, peptide mass tolerance: 1.2 Da, fragment mass tolerance: 0.6 Da).

against mouse IgG; Zymed Laboratories) for 60 min at room temperature. Phosphorylated proteins were detected by the ECL Plus method (GE Healthcare) and the immunoreactive spots were recorded on X-ray film (Hyperfilm^{TM} ECL). Only a few protein spots were detected with anti-phosphotyrosine antibodies, indicating that tyrosine phosphorylation is not a major signaling pathway in plants (Fig. 1B). A series of proteins with comparable molecular weights and different p*I* values reacted strongly with the antibodies. Other spots generated relatively weak signals. In contrast, immunodetection using the same antibodies usually finds hundreds of spots from the same amount of protein extracted from human cell lines.

The blocking activity of the N-102 solution was so effective that the background signal during immunodetection was very low. The membrane, which was used for immunodetection, was washed with water for 10 min, 50% methanol/7% acetic acid solution twice for 30 min, and again with water for five repetitions at 2 min each, and stained with colloidal gold to visualize the protein spots (Fig. 1C). 2-D PAGE patterns shown in Fig. 1A and C were similar without significant loss of spots, although intensity of each spot changed to some extent. Sufficient washing with 50% methanol/7% acetic acid solution afforded excellent staining efficiency of proteins with colloidal gold. Blocking of exposed membrane surface with proteins or polymers was necessary to minimize nonspecific binding of the antibody to the membrane. Duong and Chang [7] reported that membranes blocked with nonfat dry milk could be counterstained with colloidal gold after air-drying overnight. Ducret *et al.* [9] used PVP-40 as the blocking agent when staining proteins with colloidal gold after immunodetection. However, the blocking of N-102 usually gave better staining than that exhibited by either PVP-40 or dry milk. Membranes blocked with dry milk or BSA gave higher background by the detection with colloidal gold staining. Spots 1–3 in Fig. 1C, which correspond to the same spots in Fig. 1B, were cut out and digested with trypsin. The excised pieces of PVDF membrane were washed with 200 μL of 50 mM NH_4HCO_3/10% acetonitrile, and proteins on the membrane were digested with 10 μL of 6 ng/μL trypsin in 50 mM NH_4HCO_3. The digests were analyzed on a nanoLC-ESI-Q-TOF mass spectrometer. Peptides were separated by reverse-phase chromatography using nano flow column (50 mm × 0.15 mm id or 150 mm × 0.075 mm id) and ionized by ESI. MSMS survey mode of Q-Tof was used for data-dependent acquisition of MSMS. The raw data was converted into a pkl file using MASSLYNX software. Proteins in the digest were identified by Mascot search. Significance threshold used for protein identification was default ($p<0.05$). Each of these spots contained fructose-bisphosphate aldolase (ALF_ORYSJ). The observed shift in the p*I* of this protein suggests that it may have been phosphorylated at multiple sites. To date, however, no studies have reported on tyrosine phosphorylation of rice proteins, except the report by Hung *et al.* [12]. Conversely, human aldolase was phosphorylated at Tyr204 (201-RCQYVTE-207, ALDOA_HUMAN) [13]. As the tyrosine residue at the homologous site in the rice was conserved (196-RCAYVSE-202, ALF_ORYSJ), this site may have been phosphorylated by a dual-specificity STY kinase. Multiple spots, consisting of rice aldolase, reacted with the anti-phosphotyrosine antibody. Human aldolase was phosphorylated at Ser46, Thr65, Thr241, Thr253, Ser354, and Ser356 [14, 15]. Rice aldolase may also be phosphorylated by Ser/Thr kinases, which produce plural forms that can be separated by isoelectric focusing.

We performed differential analysis of Tyr-phosphorylation in two ovarian cancer cell lines (Fig. 2). For the differential analysis of proteins detected with antibody, spot identification requires precise matching of spots visualized with total protein detection such as CBB or colloidal gold staining. We used total protein map for two cell lines stained with CBB as a guide map and identified protein spots differentially phosphorylated. Figure 2C and D shows each part of 2-D PAGE images of two ovarian cancer cell lines detected with phosphotyrosine-specific

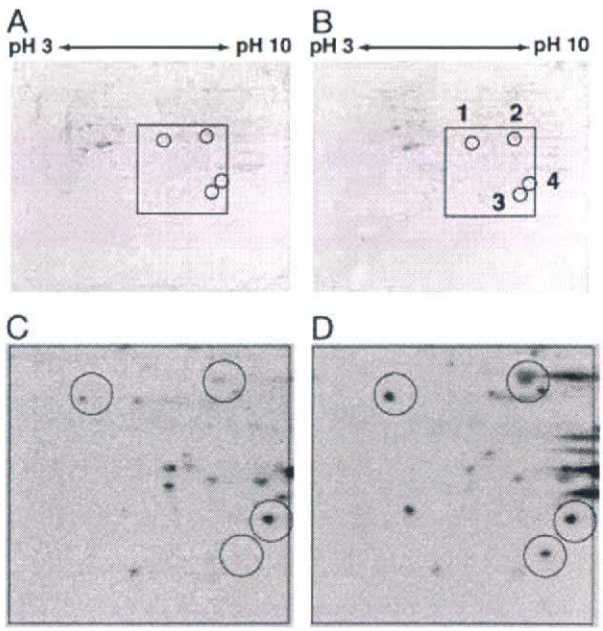

Figure 2. Differential analysis of Tyr-phosphorylated proteins between two ovarian cancer cell lines. Proteins extracted from two cell lines established from ovarian cancer were separated by 2-D PAGE and transferred to PVDF membrane. After immunodetection with phosphotyrosine-specific antibody (P-Tyr-100), the PVDF membrane was stained with CBB. (A and C) MCAS, a cell line established from ovarian mucinous cystadenocarcinoma. (B and D) OVISE, a cell line established from metastatic ovarian clear cell adenocarcinoma. (A and B) Proteins were visualized with CBB. (C and D) Immunodetection of Tyr-phosphorylated proteins. The regions indicated with boxes in A and B were shown. Circles indicate the positions of protein spots, which increased in OVISE. Spots 1–4 were identified as *S*-adenosyl-L-homocysteine hydrolase (SAHH_HUMAN), alpha-enolase (ENOA_HUMAN), carbonic anhydrase 2 (CAH2_HUMAN), and guanine nucleotide-binding protein subunit beta 2-like 1 (GBLP_HUMAN), respectively by spot digestion and MS/MS ion search of Mascot (database: SwissProt 55.2, taxonomy: *Homo sapiens*, enzyme: trypsin, peptide mass tolerance: 1.2 Da, fragment mass tolerance: 0.6 Da).

antibody. We identified four spots whose phosphorylation increased in OVISE, a cell line established from ovarian clear cell adenocarcinoma. They are shown by circles in Fig. 2C and D. Corresponding spots stained with CBB were shown in Fig. 2A and B. Proteins in these spots were digested and analyzed with nanoLC-MSMS. Spots 1, 2, 3, and 4 were identified as *S*-adenosyl-l-homocysteine hydrolase (SAHH_HUMAN), alpha-enolase (ENOA_HUMAN), carbonic anhydrase 2 (CAH2_HUMAN), and guanine nucleotide-binding protein subunit beta 2-like 1 (GBLP_HUMAN), respectively. Although we could not determine the sites of Tyr-phosphorylation of these proteins by MS analysis of the digests of protein spots, the sites of these proteins except CANH2_-HUMAN have been already reported. SAHH_HUMAN is reported to be phosphorylated at Tyr192 [16], ENOA_HUMAN is at Tyr 43, Tyr57, and Tyr287 [13, 14], and GBLP_HUMAN is at Tyr228 [13]. Identification of upstream kinase and mechanism for up-regulation of phosphorylation at these sites in ovarian clear cell adenocarcinoma cell line are under investigation.

Immunodetection of proteins separated by 2-D PAGE with group-specific antibodies is a powerful technique for focused proteomics. However, further analysis and identification typically requires additional gels or membranes. Blocking nonspecific adsorption of antibodies with the novel reagent N-102 enabled multiplex analyses, immunodetection, total protein visualization, and protein identification by MS, of proteins transferred to a PVDF membrane. This technique enabled precise differential analysis of proteins detected by the antibody.

References

[1] Gorg, A., Weiss, W., Dunn, M. J., *Proteomics* 2004, *4*, 3665–3685.

[2] Meyer, T. S., Lamberts, B. L., *Biochim. Biophys. Acta* 1965, *107*, 144–145.

[3] Berggren, K., Chernokalskaya, E., Steinberg, T. H., Kemper, C. *et al.*, *Electrophoresis* 2000, *21*, 2509–2521.

[4] Towbin, H., Staehelin, T., Gordon, J., *Proc. Natl. Acad. Sci USA* 1979, *76*, 4350–4354.

[5] Salinovich, O., Montelaro, R. C., *Anal. Biochem.* 1986, *156*, 341–347.

[6] Kemper, C., Berggren, K., Diwu, Z., Patton, W. F., *Electrophoresis* 2001, *22*, 881–889.

[7] Duong, P. T., Chang, F. N., *Electrophoresis* 2001, *22*, 2098–2102.

[8] Chevallet, M., Procaccio, V., Rabilloud, T., *Anal. Biochem.* 1997, *251*, 69–72.

[9] Ducret, A., Desponts, C., Desmarais, S., Gresser, M. J., Ramachandran, C., *Electrophoresis* 2000, *21*, 2196–2208.

[10] Wittmann-Liebold, B., Graack, H. R., Pohl, T., *Proteomics* 2006, *6*, 4688–4703.

[11] Rudrabhatla, P., Reddy, M. M., Rajasekharan, R., *Plant Mol. Biol.* 2006, *60*, 293–319.

[12] Hung, W.-C., Huan, D. D., Chien, P. S., Yeh, C. M. *et al.*, *Chemosphere* 2007, *69*, 55–62.

[13] Rush, J., Moritz, A., Lee, K. A., Guo, A. *et al.*, *Nat. Biotechnol.* 2005, *23*, 94–101.

[14] Molina, H., Horn, D. M., Tang, N., Mathivanan, S., Pandey, A., *Proc. Natl. Acad. Sci. USA* 2007, *104*, 2199–2204.

[15] Olsen, J. V., Blagoev, B. V., Gnad, B., Macek, B. *et al.*, *Cell* 2006, *127*, 635–648.

[16] Rikova, K., Guo, A., Zeng, Q., Possemato, A. *et al.*, *Cell* 2007, *131*, 1190–1203.

A Signaling Polypeptide Derived from an Innate Immune Adaptor Molecule Can Be Harnessed as a New Class of Vaccine Adjuvant[1]

Kouji Kobiyama,[3]* Fumihiko Takeshita,[2,3]* Ken J. Ishii,[†§] Shohei Koyama,[‡§] Taiki Aoshi,[†] Shizuo Akira,[‡§] Asako Sakaue-Sawano,[¶] Atsushi Miyawaki,[¶] Yuko Yamanaka,[‖] Hisashi Hirano,[‖] Koichi Suzuki,[#] and Kenji Okuda*

Modulation of intracellular signaling using cell-permeable polypeptides is a promising technology for future clinical applications. To develop a novel approach to activate innate immune signaling by synthetic polypeptides, we characterized several different polypeptides derived from the caspase recruitment domain (CARD) of IFN-β promoter stimulator 1, each of which localizes to a different subcellular compartment. Of particular interest was, N′-CARD, which consisted of the nuclear localization signal of histone H2B and the IFN-β promoter stimulator 1CARD and which localized to the nucleus. This polypeptide led to a strong production of type I IFNs and molecular and genetic analyses showed that nuclear DNA helicase II is critically involved in this response. N′-CARD polypeptide fused to a protein transduction domain (N′-CARD-PTD) readily transmigrated from the outside to the inside of the cell and triggered innate immune signaling. Administration of N′-CARD-PTD polypeptide elicited production of type I IFNs, maturation of bone marrow-derived dendritic cells, and promotion of vaccine immunogenicity by enhancing Ag-specific Th1-type immune responses, thereby protecting mice from lethal influenza infection and from outgrowth of transplanted tumors in vivo. Thus, our results indicate that the N′-CARD-PTD polypeptide belongs to a new class of vaccine adjuvant that directly triggers intracellular signal transduction by a distinct mechanism from those engaged by conventional vaccine adjuvants, such as TLR ligands. *The Journal of Immunology,* **2009, 182: 1593–1601.**

Accumulating evidence from basic research and from clinical studies clearly indicates that type I IFNs are key to the elimination of viral infection (1, 2), suppression of tumor progression (3, 4), and to vaccine immunogenicity (5). Type I IFNs, such as IFN-α and -β, are produced from a wide variety of cell types upon viral infection or in response to foreign nucleic acids, such as DNA and RNA (6–8). Recent research has dissected and elucidated the molecular basis of the ability of the immune system to sense a variety of nucleic acids as pathogen-associated molecular patterns (9) or to sense the presence of aberrant self-DNA under dangerous situations (10, 11). RIG-I-like helicases (RLHs)[4] mediate innate immune signaling in human cells induced by immunostimulatory RNAs, such as 5′-triphosphate RNA or dsRNA, or right-handed B-form DNA (B-DNA) (12–14). RLHs trigger cellular signaling through adaptor molecules, such as IFN-β promoter stimulator 1 (IPS-1, also known as MAVS/VISA/Cardif), TNFR-associating factor (TRAF) 3, and TRAF family member-associated NF-κB activator (TANK), thereby coordinating the activation of IκB kinase (IKK) family members, such as NF-κB essential modulator, IKK-α, IKK-β, TANK-binding kinase 1 (TBK1), and inducible IKK (IKKi). Once activated by such cytoplasmic kinases, NF-κB, IFN regulatory factor 3 (IRF3), and IRF7 transmigrate into the nucleus and act as master regulators of type I IFN-related gene promoters (15).

These signaling molecules contain distinct domains, and thereby associate with specific target molecules and modulate downstream signal transmission. IPS-1 plays a central role in this signaling pathway and its caspase recruitment domain (CARD) forms the death domain fold, which is structurally similar to domains of Fas-associated via death domain and caspase family members (16). The CARD of IPS-1 is essential for signal transmission through homotypic interactions with the CARDs of upstream RLHs (9). Mitochondrial sorting of IPS-1 is also crucial for its canonical

*Department of Molecular Biodefense Research, Yokohama City University Graduate School of Medicine, Yokohama, Japan; †Department of Molecular Protozoology and ‡Host Defense, Research Institute for Microbial Diseases, Osaka University, Suita, Japan; §World Premier International Immunology Frontier Research Center, Osaka University, Suita, Japan; ¶Laboratory for Cell Function Dynamics, Advanced Technology Development Group, Brain Science Institute, RIKEN, Wako, Japan; ‖Kihara Institute for Biological Research, Yokohama City University Graduate School of Integrated Science, Totsuka, Japan; and #Department of Bioregulation, National Institute of Infectious Diseases, Higashimurayama-shi, Japan

Received for publication July 24, 2008. Accepted for publication November 19, 2008.

The costs of publication of this article were defrayed in part by the payment of page charges. This article must therefore be hereby marked *advertisement* in accordance with 18 U.S.C. Section 1734 solely to indicate this fact.

[1] This work was supported, in part, by the Strategic Research Project of Yokohama City University (K18022 to F.T.), the Advancement of Medical Sciences from Yokohama Medical Foundation (to F.T. and K.K.), the National Institute of Biomedical Innovation (to K.O.), the Yasuda Medical Foundation (to F.T.), the Uehara Memorial Foundation (to F.T.), and a Grant-in-aid for Scientific Research (20590477 to F.T.) from the Ministry of Education, Culture, Sports, Science, and Technology of Japan.

[2] Address correspondence and reprint requests to Dr. Fumihiko Takeshita, Department of Molecular Biodefense Research, Yokohama City University Graduate School of Medicine, 3-9 Fukuura, Kanazawaku, Yokohama, Japan. E-mail address: takesita@yokohama-cu.ac.jp

[3] K.K. and F.T. contributed equally to this work.

[4] Abbreviations used in this paper: RLH, RIG-I-like helicase; B-DNA, B-form DNA; IPS-1, IFN-β promoter stimulator 1; TRAF, TNFR-associating factor; TANK, TRAF family member-associated NF-κB activator; TBK1, TANK binding kinase 1; IKK, IκB kinase; IKKi, inducible IKK; IRF3, IFN regulatory factor 3; CARD, caspase recruitment domain; N′-CARD, fusion of the NH_2-terminal nuclear localization signal of histone H2B to the IPS-1 CARD; PTD, protein transduction domain; TMD, transmembrane domain; NLS, nuclear localization signal; NDH, nuclear DNA helicase II; ODN, oligodeoxynucleotide; flu vax, influenza split-product vaccine; DC, dendritic cell; FL, full length; BM-DC, bone marrow-derived dendritic cell.

signaling because human hepatitis C virus NS3/4A protease inactivates IPS-1 by cleaving a region adjacent to the transmembrane domain (TMD), which is required for IPS-1 localization to the mitochondrial outer membrane (17).

To develop a novel approach to modulate innate immune signaling by synthetic polypeptides, we generated several different IPS-1 CARD-fusion polypeptides, each of which localizes to a different subcellular compartment. Of interest, the nuclear localization of a fusion polypeptide between the nuclear localization signal (NLS) of histone H2B and the IPS-1 CARD (hereafter referred to as N′-CARD) activated a distinct signaling pathway initiated from the nucleus and led to a strong production of type I IFN. Molecular and genetic analyses showed that nuclear DNA helicase II (NDH) is critically involved in this signaling pathway. Fusion of N′-CARD to the protein transduction domain (PTD), originally derived from the HIV Tat protein (18), facilitated transduction of N′-CARD from outside to inside the cell without loss of its original intracellular function. Finally, we demonstrate that the N′-CARD-PTD polypeptide acts as a novel vaccine adjuvant by directly triggering innate intracellular immune signaling to augment vaccine immunogenicity. Such a mechanism is distinct from TLR-mediated signaling, which is engaged in innate immune activation by conventional vaccine adjuvants, such as monophosphoryl-lipid A (an LPS derivative) and CpG oligodeoxynucleotide (ODN).

Materials and Methods

Cells and reagents

HEK293, HeLa, RAW264.7, and TC-1 cells were purchased from American Type Culture Collection and maintained in DMEM supplemented with 10% FCS and 50 μg/ml penicillin/streptomycin. Sf9 cells were maintained in Sf900 II SFM (Invitrogen). LPS was purchased from Sigma-Aldrich. CpG ODN, 5′-ATC GAC TCT CGA GCG TTC TC-3′, was synthesized by Gene Design. Mouse GM-CSF and Flt3L were purchased from PeproTech. Influenza split-product vaccine (flu vax) was prepared at The Research Foundation for Microbial Diseases of Osaka University (Kanon-ji city, Kagawa, Japan) from the purified influenza virus A/New Caledonia/20/99 strain (H1N1) by sequential treatment with ether and formalin, according to the method of Davenport et al. (19, 20).

Expression plasmids

The IPS-1 expression plasmid was described previously (21). The IPS-1 CARD, aa 1–100 of the IPS-1 ORF, was PCR-amplified. Fusion cDNAs were generated by ligating aa 1–100 and 514–540 of IPS-1 ORF (CARD-TMD), aa 1–37 of histone H2B ORF and aa 1–100 of IPS-1 ORF (N′-CARD), N′-CARD and aa 514–540 of hIPS-1 ORF (N′-CARD-TMD), and were amplified by PCR. These fragments were introduced in-frame into pFLAG CMV5b (Sigma-Aldrich) or pGEX6P-2 (GE Healthcare). GST-N′-CARD was further fused to the PTD (Tyr-Ala-Arg-Ala-Ala-Ala-Arg-Gln-Ala-Arg-Ala) and introduced into pFastBac HT-B (Invitrogen). TBK1, IKKi, NDH, and chloride channel 1A (CC1A) cDNAs were amplified by PCR using a human spleen cDNA library (Takara). These fragments were introduced in-frame into pFLAG-CMV4 (Sigma-Aldrich), pCIneo-HA, pCAGGS-Flag-m1SECFP, pCAG-His Venus, or pcDNA3-RFP. The N′-CARD T54A expression plasmid was generated by site-directed mutagenesis, as described previously (22). The sequences of the PCR products were confirmed using an ABI PRISM Genetic Analyzer (PE Applied Biosystems).

Luciferase assay

The luciferase assay was conducted as described previously (23).

Confocal microscopy

HeLa cells were transfected with CARD-YFP, CARD-TMD-YFP, N′-CARD-YFP, N′-CARD-TMD-YFP, IPS-1-YFP, YFP-IKKi, YFP-TBK1, and/or mRFP-NDH and incubated for 48 h. In some cases, the cells were treated with Hoechst 33258 (Invitrogen) and/or MitoTracker reagent (Invitrogen) at 37°C for 15 min. Alternatively, HeLa cells were treated with CARD or N′-CARD-PTD for 30 min. Cells were treated with Hoechst 33258 for 15 min before fixation and incubation with mouse anti-FLAG M2-Cy3. After washing with PBS containing 1% BSA, the cells were examined under an FV 500 confocal microscope (Olympus).

Immunoprecipitation and immunoblotting

Immunoprecipitation and immunoblotting was performed as described previously (24) using anti-FLAG M2 (Sigma-Aldrich), anti-FLAG M2-HRP (Sigma-Aldrich), anti-HA (Covance), anti-HA-HRP (Roche Diagnostics), anti-ubiquitin-HRP (Santa Cruz Biotechnology), anti-NDH (provided by J. D. Parvin, Brigham and Women's Hospital, Boston, MA), anti-p-JNK, anti-p-p38, anti-p-ERK, and anti-β-actin (Cell Signaling Technology).

RNA interference

An siRNA targeting NDH mRNA (stealth RNAi) was chemically synthesized by Invitrogen (Carlsbad, CA): sense, 5′-AUU GCU UGC AAA UCA UGA UCC UGU U-3′; antisense, 5′-AAC AGG AUC AUG AUU UGC AAG CAA U-3′. HEK293 cells (6×10^5) were transfected with 120 pmol of control or NDH siRNA using Lipofectamine RNAi MAX reagent (Invitrogen) according to the manufacturer's protocol.

Purification of recombinant polypeptides

DH10Bac competent cells (Invitrogen) were transformed with pFastBac HT-B-GST or with GST-N′-CARD-PTD to generate recombinant Bacmids. Sf9 cells were transfected with Bacmid-encoding GST or GST-N′-CARD-PTD to generate recombinant seed baculoviruses. Seventy-two hours after infection, the Sf9 cells were washed once with PBS and suspended in sonication buffer (50 mM Tris-HCl (pH 8.0), 50 mM NaCl, 1 mM EDTA, 1 mM DTT) containing 10% Triton X-100. After sonication, cell lysates were centrifuged at 15,000 rpm, at 4°C for 30 min. The supernatants were collected and dialyzed with sonication buffer. Recombinant polypeptides were purified using GSTrap (GE Healthcare) according to the manufacturer's protocol. In brief, after the column was equilibrated with 2 ml sonication buffer, the cell lysate was applied and the column then washed three times with 10 ml PBST (PBS containing 0.5% Triton X-100) and with PBS once. Recombinant polypeptide (GST or GST-N′-CARD-PTD) was eluted with sonication buffer containing 10 mM reduced glutathione and then dialyzed with PBS. Recombinant proteins (1 μg) used in all the experiments contained <20 fg endotoxins (*Limulus* J Single Test, Wako).

ELISA and RT-PCR

Bone marrow-derived dendritic cells (DCs) were generated by 5 days of culture with GM-CSF (20 ng/ml) (GM-DCs) or Flt3L (100 ng/ml) (FL-DCs). GM-DCs or FL-DCs were treated with or without 1, 3, or 10 μg/ml N′-CARD-PTD or 1 μM of CpG ODN for 24 h and the supernatants were subjected to ELISA for mouse IFN-α, IFN-β (PBL Biomedical Laboratories), or IL-12 p40 (Invitrogen). RAW264.7 cells were treated with 1 μg/ml LPS or 10 μg/ml N′-CARD-PTD for 3, 6, 12, 18, 24, and 48 h. The levels of mRNA for TNF-α, IL-6, IFN-α, IFN-β, IP-10, and β-actin were examined by RT-PCR as described previously (5, 22).

Immunization

Eight-week-old female BALB/c mice were administered s.c. with N′-CARD-PTD (5 μg), CpG ODN (5 μg), or flu vax (0.7 μg) alone, flu vax (0.7 μg) plus N′-CARD-PTD (5 μg), or flu vax (0.7 μg) plus CpG ODN (5 μg) at 0 and 10 days. Blood was drawn at 20 days and serum Ab titer was measured by ELISA as described previously (25). Alternatively, 8-wk-old female C57BL/6 mice were immunized with E7 peptide (E7, Arg-Ala-His-Tyr-Asn-Ile-Val-Thr-Phe, 3 μg), E7 plus N′-CARD-PTD (5 μg), or E7 plus CpG ODN (5 μg) at 0 and 2 wk. Splenocytes were harvested 2 wk after final immunization. The cells were incubated with 1 μg/ml E7 or NP peptide (Ala-Ser-Asn-Glu-Asn-Met-Glu-Thr-Met) for 18 h at 37°C. Total RNA was isolated and real-time PCR was performed as described previously (22).

Influenza challenge

Ten days after final immunization, mice were challenged intranasally with 2×10^4 pfu (8 LD_{50}) of influenza virus A/PR/8/34 (25). The body weights and mortality of the challenged mice were monitored for the next 14 days.

Tumor transplantation

Eight week-old C57BL/6 mice were administered subcutaneously with TC-1 (1×10^5 cells/mouse), a mouse lung carcinoma expressing E7 Ag (25). Mice were immunized with control NP peptide (3 μg), E7 (3 μg), N′-CARD-PTD (5 μg), or E7 (3 μg) plus N′-CARD-PTD (5 μg) at 3, 4, 5, 6, and 7 day after TC-1 inoculation. The sizes of local tumor mass were monitored for the next 20 days.

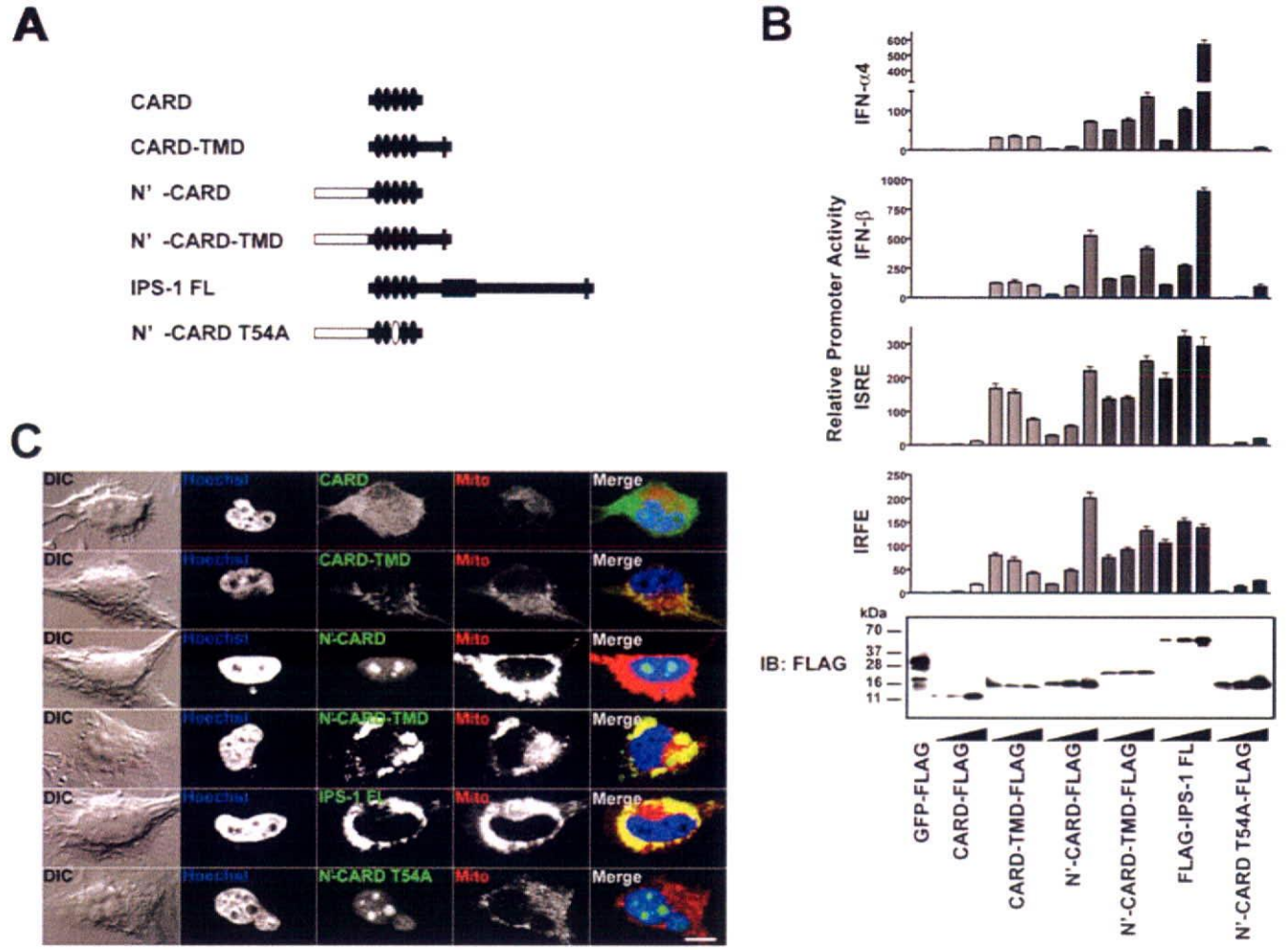

FIGURE 1. Synthetic IPS-1 CARD fusion molecules induce activation of type I IFN-related promoters. *A*, Schematic diagram of synthetic fusion molecules consisting of domains derived from IPS-1 and histone H2B. *B*, HEK293 cells were transfected with the expression plasmids, GFP-FLAG, CARD-FLAG, CARD-TMD-FLAG, N′-CARD-FLAG, N′-CARD-TMD-FLAG, FLAG-IPS-1 FL, and N′-CARD T54A-FLAG in the presence of TK-RL plus a reporter plasmid expressing firefly luciferase under the control of either the IFN-α4 promoter (*top panel*), the IFN-β promoter (*second panel from the top*), the ISRE-dependent promoter (*third panel from the top*), or the IRFE-dependent promoter (*fourth panel from the top*). Data represent means ± SD of the relative luciferase activity of six samples. Cell lysates were also subjected to immunoblot analysis to examine levels of target polypeptide expression (*bottom panel*). *C*, HeLa cells were transfected with the expression plasmids, YFP-CARD, YFP-CARD-TMD, YFP-N′-CARD, YFP-N′-CARD-TMD, YFP-IPS-1 FL, and YFP-N′-CARD T54A. Genomic DNA or mitochondria were stained with Hoechst 33258 or Mitotracker reagent, respectively, and then analyzed under a confocal microscope. The data represent one of three independent experiments with similar results. Scale bar, 10 μm.

Statistical analysis

The Student's *t* test or the Mantel-Cox log rank test was used for statistical analysis.

Results

The nuclear redistribution of IPS-1 CARD elicits type I IFN promoter activation

To elucidate the mechanisms underlying IPS-1 CARD-mediated signaling, plasmids encoding either the IPS-1 CARD alone or the IPS CARD fused to the IPS-1 TMD or to the NLS of histone H2B were generated and their abilities to induce type I IFN-related promoter activation were characterized (Fig. 1*A*). Although the CARD alone had minimal activity in eliciting such promoter activation, fusion of the TMD to the CARD (CARD-TMD) resulted in a significant activation, suggesting that the TMD facilitates CARD-mediated signaling, consistent with previous data (Fig. 1*B*; Ref. 26). Of interest, fusion of the NH_2-terminal NLS of histone H2B to the IPS-1 CARD (N′-CARD) conferred strong promoter activation, suggesting that nuclear localization of N′-CARD triggers signal activation. Indeed, N′-CARD induced phosphorylation of IRF3 at a comparable level to full length IPS-1 (FL) (Supplemental Fig. 1).[5] The mutant polypeptide N′-CARD T54A, in which the third α-helical structure of the CARD was disrupted (22), induced significantly lower levels of promoter activation, suggesting that the conformation of the IPS-1 CARD is also critical for its activity. Although N′-CARD fused to the IPS-1 TMD (N′-CARD-TMD) induced significant levels of promoter activation, the levels were comparable to those induced by N′-CARD or CARD-TMD, suggesting that the effects of CARD distribution mediated by the NLS and the IPS-1 TMD are redundant.

N′-CARD localizes to the nucleus and signals through NDH

To elucidate the signaling mechanisms triggered by N′-CARD and CARD-TMD, we examined the subcellular localizations of these fusion molecules. Confocal microscopy analysis showed that CARD-TMD fused to YFP (YFP-CARD-TMD) was present in

[5] The online version of this article contains supplemental information.

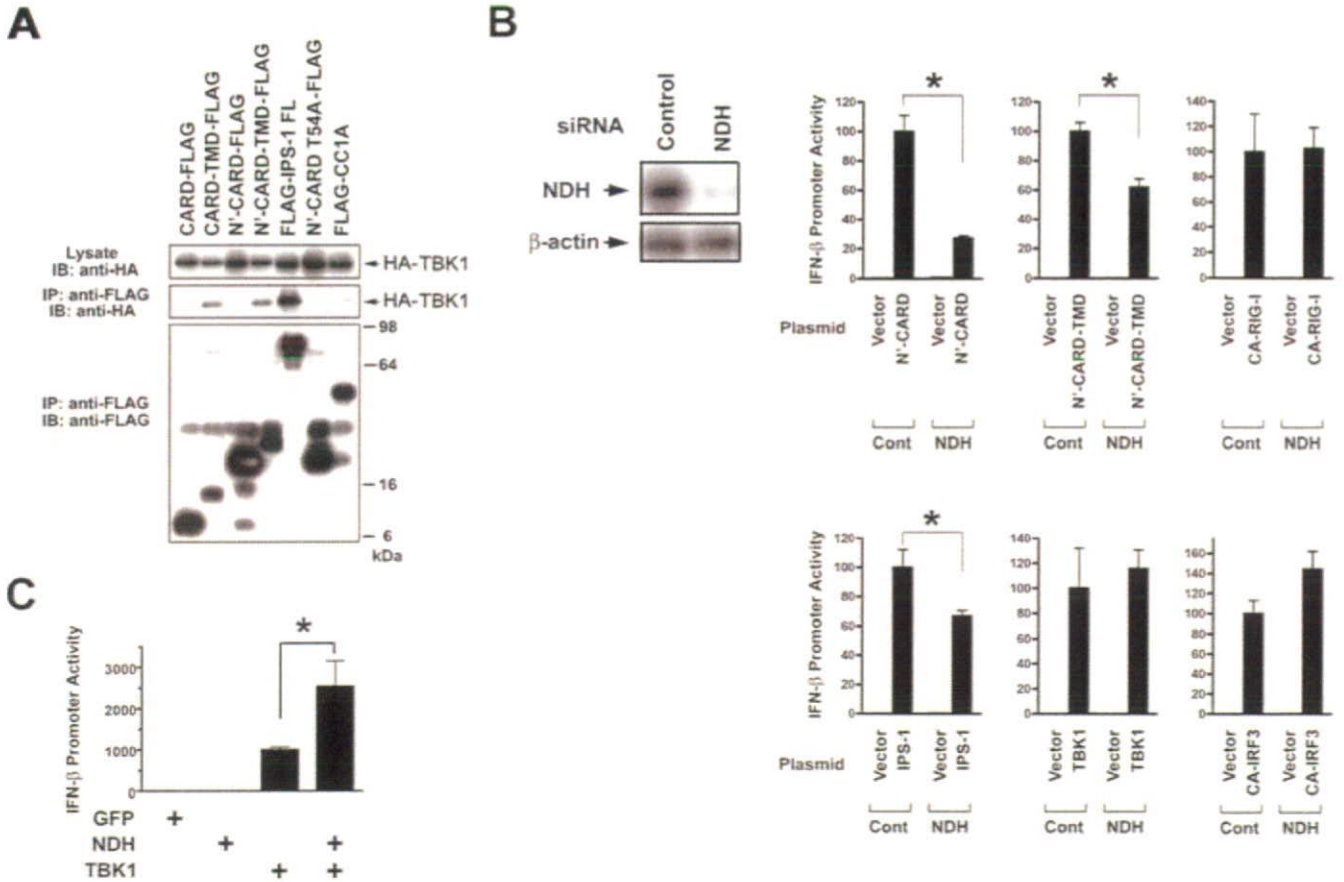

FIGURE 2. Role of NDH in N′-CARD-mediated signaling. *A*, Cell lysates from HEK293 cells transfected with the expression plasmids for HA-TBK1 plus CARD-FLAG, CARD-TMD-FLAG, N′-CARD-FLAG, N′-CARD-TMD-FLAG, FLAG-IPS-1 FL, N′-CARD T54A-FLAG, or FLAG-CC1A were prepared and immunoprecipitated with anti-FLAG Ab. The immune complexes were analyzed by immunoblotting using anti-HA or anti-FLAG Ab. *B*, After HEK293 cells were transfected with control or NDH siRNA, the levels of NDH protein were examined by immunoblotting. The cells were further transfected with the expression plasmid for N′-CARD, N′-CARD-TMD, CA-RIG-I, IPS-1, TBK1, and CA-IRF3 in the presence of TK-RL plus a reporter plasmid expressing firefly luciferase under the control of the IFN-β promoter. *C*, HEK293 cells were transfected with the expression plasmid(s) for GFP, NDH, and/or TBK1 in the presence of TK-RL plus a reporter plasmid expressing firefly luciferase under the control of the IFN-β promoter. *B* and *C*, Forty eight hours after transfection, luciferase assay was performed. Data represent means ± SD of the relative luciferase activity of eight samples. *, $p < 0.05$.

mitochondria, with a localization pattern similar to that of IPS-1 FL (YFP-IPS-1 FL), while N′-CARD fused to YFP (YFP-N′-CARD) was mostly present in the nuclear interchromosomal space (Fig. 1*C*). Because CARD alone (YFP-CARD) was present diffusely within the cell and both YFP-N′-CARD and YFP-N′-CARD T54A localized to the nucleus, it was suggested that the NLS directed the nuclear distribution of the IPS-1 CARD (Fig. 1*C*). These results implied that N′-CARD triggers cellular signaling pathways that originate in the nucleus and that are distinct from those triggered by CARD-TMD or IPS-1 FL, which originate from mitochondria.

TBK1, and its closely related IKK family member IKKi, are kinases acting downstream of IPS-1 and are required for a type I IFN production (21, 26, 27). We next examined the molecular interactions between each CARD-fusion molecule and TBK1 by immunoprecipitation analysis. As a control, TBK1 was coprecipitated with IPS-1 FL (Fig. 2*A*). A significant amount of TBK1 was also detected after precipitation with CARD-TMD or N′-CARD-TMD, but not after precipitation with CARD, N′-CARD, or N′-CARD T54A, suggesting that the TMD supports the association of the CARD with TBK1 (Fig. 2*A*).

To examine the signaling mechanisms triggered by N′-CARD, we tried to identify cellular molecules that associate with N′-CARD using a tandem-affinity purification system and TOF-MS analysis (data not shown). Among the N′-CARD interacting molecules identified, we were particularly interested in nuclear DNA helicase II (NDH, also known as RNA helicase A), a 1270 amino acid protein containing two copies of a dsRNA binding domain, a DEIH (Asp-Glu-Ile-His) helicase core, and an RGG (Arg-Gly-Gly) box nucleic acid-binding domain.

To examine the functional role of NDH in the signaling pathway leading to type I IFN production, NDH mRNA was ablated by RNA interference. Endogenous NDH protein was specifically decreased by NDH siRNA but not by control siRNA treatment (Fig. 2*B*). Knockdown of NDH resulted in a suppression of N′-CARD-induced IFN-β promoter activation by 73%. The level of promoter activation induced by IPS-1 or N′-CARD-TMD was also partially suppressed in NDH-knockdown cells by 33 and 38%, respectively. The levels were comparable when a constitutively active form of RIG-I (RIG-I 2CARDs), TBK1, or a constitutively active form of IRF3 (IRF3CA) was examined (Fig. 2*B*). Although over-expression of NDH had no effect, and over-expression of TBK-1 had a minimal effect on IFN-β promoter activation, over-expression of NDH plus TBK1 synergistically activated the IFN-β promoter, suggesting that NDH had the ability to up-regulate TBK1 activity (Fig. 2*C*). These results, taken together, suggest that NDH is involved in the events downstream of N′-CARD, and partially in

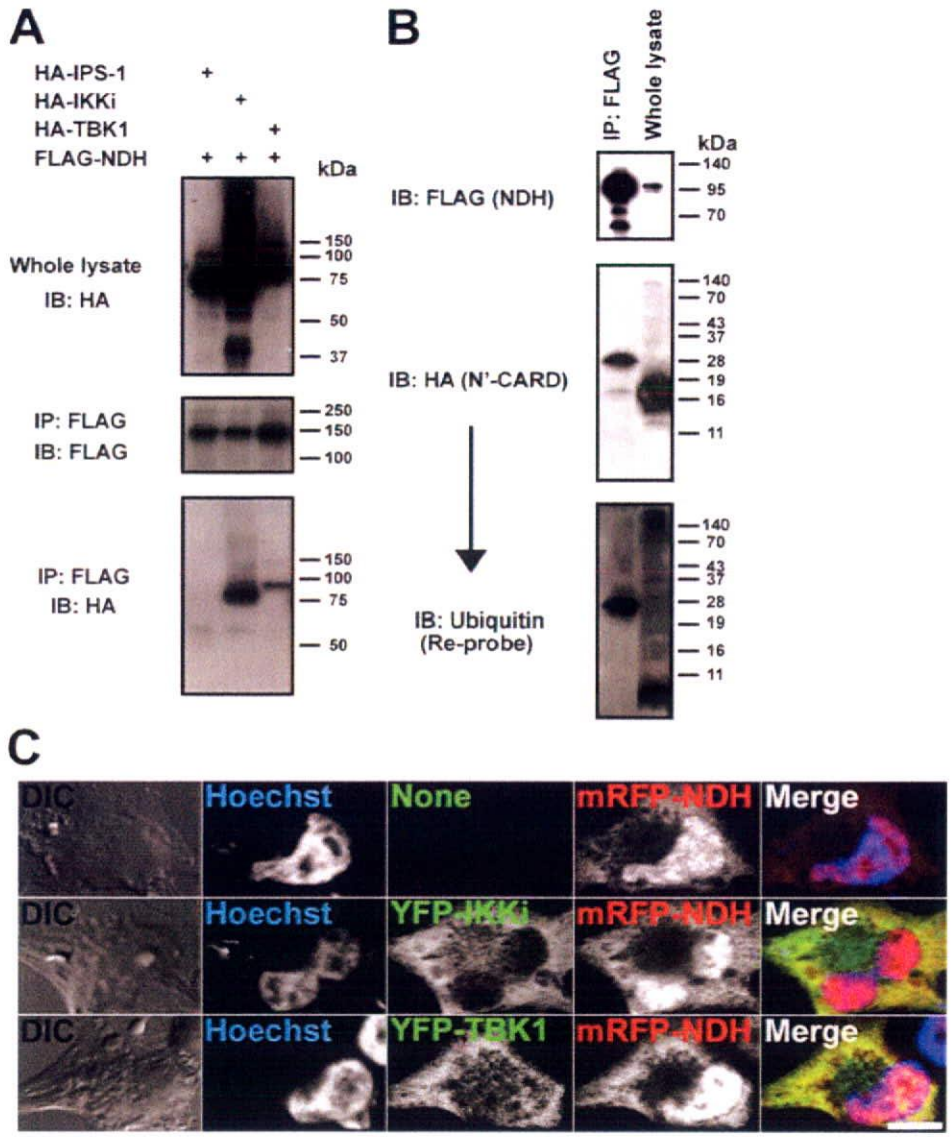

FIGURE 3. NDH associates with N′-CARD, TBK1, and IKKi. *A* and *B*, The lysates of HEK293 cells transfected with the expression plasmids for FLAG-NDH plus HA-IPS-1, HA-IKKi, HA-TBK1 (*A*) or N′-CARD-HA (*B*) were prepared and immunoprecipitated with anti-FLAG Ab. The immunoblots were probed with anti-HA or anti-FLAG Ab (*A* and *B*) or sequentially probed with anti-HA and anti-ubiquitin Ab (*B*). *C*, HeLa cells were transfected with an expression plasmid for mRFP-NDH alone or with those for mRFP-NDH and YFP-IKKi or YFP-TBK1. After staining with Hoechst 33258, the cells were examined under a confocal microscope. Data represent one of three independent experiments with similar results. Scale bar, 10 μm.

those downstream of IPS-1, and that it plays a role in signaling upstream of TBK1.

To confirm the physical interactions among NDH, IKKi, TBK1, and N′-CARD, immunoprecipitation analysis was performed. A strong interaction was detected between NDH and IKKi or TBK1, while there was no apparent association of NDH with IPS-1 in this assay (Fig. 3*A*). By contrast, NDH was confirmed to interact with N′-CARD. Of interest, the mobility of N′-CARD coprecipitated with NDH was retarded in SDS-PAGE (~25 kDa) when compared with that in whole cell lysate (~18 kDa) (Fig. 3*B*). The retarded N′-CARD was detected by anti-ubiquitin Ab, suggesting that mono-ubiquitinated N′-CARD, directly or indirectly, has the ability to associate with NDH (Fig. 3*B*). We also examined the subcellular localization of NDH, IKKi, and TBK1 by confocal microscopy analysis (Fig. 3*C*). Both YFP-IKKi and YFP-TBK1 were mostly present in the cytoplasm, while mRFP-NDH was diffusely present within the cell. Most NDH present within the cytoplasm colocalized with IKKi or TBK1 (Fig. 3*C*).

Recombinant N′-CARD polypeptide fused to the protein transduction domain (N′-CARD-PTD) induces type I IFN production and exerts innate immune responses in vitro

To examine the potent ability of N′-CARD in modulating innate immune responses, we generated a recombinant N′-CARD polypeptide fused to the PTD, which enables transduction of extracellular protein into intracellular compartments. When the N′-CARD-PTD polypeptide was added to the culture medium of HeLa cells, it entered the nucleus within 30 min (Fig. 4*A*). By contrast, when the same amount of CARD polypeptide was added, only a minimal level of the polypeptide was observed inside the cell (Fig. 4*A*). The addition of the N′-CARD-PTD polypeptide alone induced significant levels of IFN-β promoter activation in HEK293 cells, suggesting that N′-CARD-PTD has the ability to transmigrate into the cell and trigger NDH-mediated cellular signaling to elicit type I IFN production (Supplemental Fig. 2).

We next examined whether administration of the N′-CARD-PTD polypeptide activates immune cells in vitro. As shown in Fig. 4*B*, N′-CARD-PTD induced production of a proinflammatory cytokine (TNF-α), type I IFNs (IFN-α and -β), and an IFN-stimulated gene product (IP-10) in a mouse macrophage cell line, RAW264.7. The expression of IFN-α and -β mRNAs was detected within 18 h; the expression of IFN-α mRNA continued for more than 48 h after N′-CARD-PTD treatment. By contrast, LPS, an activator of TLR4-mediated innate immune responses, induced IFN-β mRNA within 3 h, but this induction lasted for less than 18 h. The overall level of IFN-α mRNA production was higher in cells stimulated with N′-CARD-PTD compared with those stimulated with LPS, while that of IFN-β was lower in those stimulated

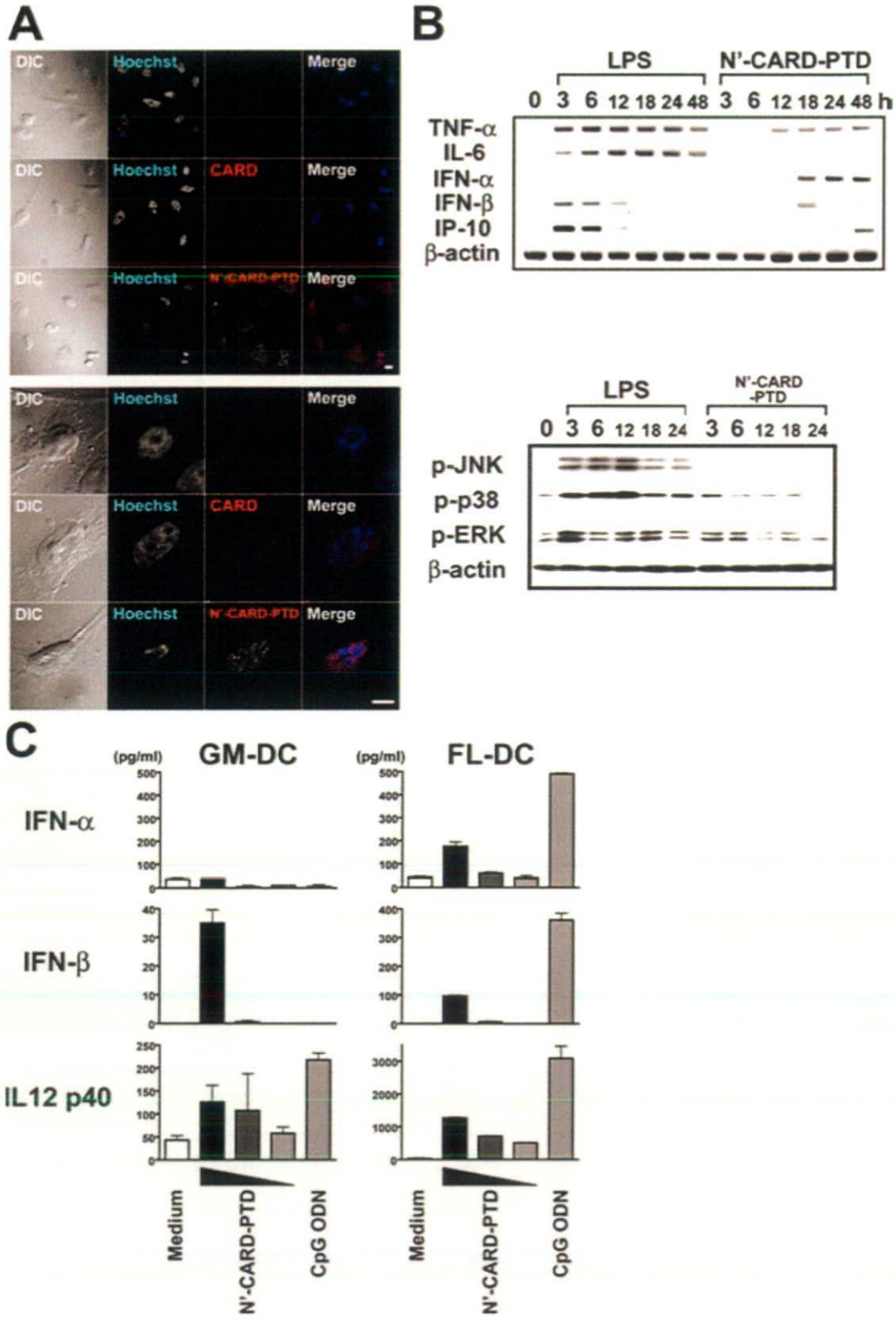

FIGURE 4. The N′-CARD-PTD polypeptide induces type I IFN production and DC maturation. *A*, Recombinant CARD or N′-CARD-PTD polypeptide was administered into the culture medium of HeLa cells. Thirty minutes after addition, the cells were permeabilized, stained with anti-FLAG M2-Cy3 and Hoechst 33258, and subjected to confocal microscopy analysis. *Upper panel,* Lower magnification. *Lower panel,* Higher magnification. Scale bar, 10 μm. *B*, RAW264.7 cells were treated with 1 μg/ml LPS or 10 μg/ml N′-CARD-PTD for 3, 6, 12, 18, 24, and 48 h. The levels of mRNA expression for TNF-α, IL-6, IFN-α, IFN-β, IP-10 and β-actin were examined by RT-PCR (*upper panel*). The levels of phosphorylated JNK, p38, or ERK were examined by immunoblotting (*lower panel*). *C*, GM-DCs or FL-DCs were treated with or without 1, 3, or 10 μg/ml N′-CARD-PTD or 1 μM of CpG ODN for 24 h and the supernatants were subjected to ELISA for mouse IFN-α, IFN-β, or IL-12 p40. Data represent one of two or three independent experiments with similar results.